JOURNAL OF GEOPHYSICAL RESEARCH, VOL. 99, NO. C1, PAGES 843–864, JANUARY 15, 1994

Numerical experiments of internal wave generation by strong tidal flow across a finite amplitude bank edge

Kevin G. Lamb

Department of Physics, Memorial University of Newfoundland, St. John's, Newfoundland, Canada

Results of some idealized numerical experiments of strong tidal flow of a stratified fluid across a finite amplitude bank edge are presented. These experiments were motivated by a need to develop an understanding of some of the complex internal wave phenomena observed on Georges Bank (Loder et al., 1992) and at other locations where tidal forcing is strong. The numerical model solves the fully nonlinear, nonhydrostatic Boussinesq equations on an f plane. The model is two-dimensional, with spatial variation in the vertical and cross-bank directions only. Model forcings are based on the Georges Bank observations. A horizontally uniform stratification is used. The model successfully reproduces some observed features including the formation of a large depression and a hydraulic jump over the bank edge during off-bank flow and two on-bank propagating depressions every tidal period. An undular bore propagating away from the bank is in agreement with other observations (La Violette et al., 1990). Rotational effects are shown to be responsible for the formation of the second of the on-bank propagating depressions. Sensitivity of the results to the topographic slope, tidal current strength, stratification, and model initialization is explored.

1. INTRODUCTION

The generation of internal gravity waves by tidal flow over topography in the ocean occurs in a variety of topographic regimes such as shelf-breaks, bank edges, and fjord sills [e.g., *Farmer and Smith*, 1980; *Pingree et al.*, 1983; *Holloway*, 1987; *Loder et al.*, 1992]. These waves have been suggested as an important source of vertical mixing for nutrients, sediments, and other water mass properties and materials [*Sandstrom and Elliott*, 1984; *Brickman and Loder*, 1993; *Huthnance*, 1989]. The northern edge of Georges Bank in the Gulf of Maine has recently been identified as a location of complex internal waves of potential significance to the Bank's high biological productivity [*Loder et al.*, 1992; see also *Marsden*, 1986; *La Violette et al.*, 1990]. Significant nonlinear current interactions associated with the strong tidal currents on Georges Bank have been identified [*Loder*, 1980; *Loder and Horne*, 1991]. Observations of internal waves generated by tidal flow in numerous localities illustrate the importance of understanding this phenomenon (see *Huthnance* [1989] for an exhaustive list).

The generation of internal gravity waves in the ocean can be complicated by many interrelated factors including nonlinearities in the governing equations, finite amplitude topography, spatially-varying tidal current strength and phase, spatially and temporally varying stratification, boundary-layer and turbulent effects, overturning waves and associated mixing, and background residual currents. In order to develop an understanding of the wave generation process in general, some idealized numerical experiments are being carried out with the northern side of Georges Bank as a focus. The goal of the first set of these is to develop an understanding of the fundamentals of the general problem of nonlinear internal wave generation due to strong tidal flow across a finite-amplitude bank edge without frictional effects. The results of these experiments for the case of a horizontally-uniform density field are contained in this paper. The model forcings are chosen appropriate to the northern Georges Bank regime, and the results are discussed in relation to the observations described by *Loder et al.* [1992] and *Brickman and Loder* [1993].

Laboratory and numerical experiments investigating stratified tidal flow over finite amplitude topography have been carried out [e.g., *Maxworthy*, 1979; *Hibiya*, 1988; *Matsuura and Hibiya*, 1990; *Willmott and Edwards*, 1987. The numerical work in *Hibiya* [1988] and *Matsuura and Hibiya* [1990], being fully nonlinear and nonhydrostatic calculations, come closest to the calculations presented here. All these studies used different topographies from that considered here and did not include rotation. Theoretical work has been restricted to the linearized, inviscid equations of motion [e.g., *Baines*, 1982; *Craig*, 1988; *Hibiya*, 1986]. Of these only *Hibiya* [1986] included advection of the waves by the tidal flow, something of crucial importance in the Georges Bank situation, but his study was in the small-obstacle hydrostatic limit and excluded rotational effects.

The outline of the paper is as follows. In section 2 the numerical method used is outlined. In section 3 the model initialization is described. The results for a base case run are described in detail in section 4. In section 5 results of other model runs are briefly described which test the effects of the Coriolis term and the model sensitivity to the tidal strength, topography, stratification and initialization of the along-bank flow. A summary and discussion of the results are found in section 6.

2. NUMERICAL MODEL

The model equations are the two-dimensional inviscid, incompressible Boussinesq equations on a rotating f plane:

$$\mathbf{U}_t + \mathbf{U}\cdot\nabla\mathbf{U} - fv\hat{\mathbf{i}} = -\nabla p - \rho\mathbf{g} \qquad (1a)$$

$$v_t + \mathbf{U}\cdot\nabla v + fu = 0 \qquad (1b)$$

Paper number 93JC02514.
0148-0227/94/93JC-02514$05.00

$$\rho_t + U\cdot\nabla\rho = 0 \tag{1c}$$

$$\nabla\cdot U = 0. \tag{1d}$$

$\mathbf{U} = (u,w)$ is the velocity vector in the cross-bank plane with u the horizontal (positive off-bank) velocity and w the vertical velocity, (x,z) are the corresponding spatial coordinates (Figure 1), ∇ is the gradient operator $(\partial/\partial x, \partial/\partial z)$ and t is time. The along-bank velocity v is included in the model, but no variation with the along-bank coordinate y is allowed. The fluid density is $1 + \rho$ and $gz + p$ is the pressure (henceforth p and ρ will be called the pressure and density, respectively), $\mathbf{g}$ is the vector $(0,g)$, where g is the gravitational acceleration, and i is the unit vector in the positive x direction. The Coriolis parameter f is taken as 10^{-4} s^{-1}.

The equations are solved on a domain bounded below by the topography at $z = h(z)$ and above by a rigid lid at $z = H$ (see Figure 1). H is the deep-water depth. The inviscid boundary conditions include no normal flow at the upper and lower boundaries. The boundary conditions at the left and right open boundaries are described below.

The model used is essentially the same as that described in *Lamb* [1993], the only differences being the forcing method, the Coriolis term and the additional equation for v. The model uses the second-order projection method developed for a homogeneous fluid by *Bell et al.* [1989*a*] and extended to a fully stratified fluid by *Bell and Marcus* [1992] and to general structured quadrilateral grids by *Bell et al.* [1989*b*]. The advantages of this method are that it works well for inviscid flows and has the ability to capture large gradients. No mixing/frictional terms are required for numerical stability. A very brief overview of the method will now be given.

The time stepping in the model is done as follows. First v and ρ are updated via

$$\frac{v^{n+1} - v^n}{dt} = -(U\cdot\nabla + fu)^{n+1/2} \tag{2}$$

and

$$\frac{\rho^{n+1} - \rho^n}{dt} = -(U\cdot\nabla\rho)^{n+1/2} \tag{3}$$

Next the vector

$$V = -(U\cdot\nabla U)^{n+1/2} - \frac{\rho^{n+1} + \rho^n}{2} g + f\frac{v^{n+1} + v^n}{2} i \tag{4}$$

is computed. Finally the vector field $\mathbf{U}$ and the pressure gradients are updated via

$$\frac{U^{n+1} - U^n}{dt} = P(V)$$
$$\nabla p^{n+1/2} = (I - P)(V) \tag{5}$$

Here P is the projection operator which projects a vector field onto its divergence free part and I is the identity operator. The flow is forced by specifying $\mathbf{U}_t$ at the left boundary. The right boundary condition requires the specification of a vector to which the vertical pressure gradient along the right boundary is weakly associated [*Bell and Marcus*, 1992]. A good choice of this vector was not found for the physical situation considered here. To circumvent this, the model domain was taken large enough to ensure that no waves hit either boundary. The convective terms and fu at the half time step $n + 1/2$ are calculated using an upwinding extrapolation procedure [*Bell et al.*, 1989*b*].

The time step is restricted by two things. First, a Courant-Friedrichs-Lewy condition must be satisfied. It requires that a fluid particle cannot travel the length of a grid cell in one time step. The maximum allowable time step is further restricted by the stiffness of the gravitational forcing [*Bell and Marcus*, 1992]. For the base case run described in section 4 a time step of 5 s was used. For the lower resolution sensitivity studies, time steps of 20 s were used.

The equations are not solved exactly as shown above. They are first transformed to a terrain following coordinate system with higher horizontal resolution over the bank edge (Figure 1), making the governing equations somewhat more complicated [*Bell et al.*, 1989*b*]. The values of $\mathbf{U}$, v, ρ and ∇p are specified at the cell centers and at the midpoints of cell edges lying along the boundaries. The latter are used to apply the boundary conditions.

3. MODEL INITIALIZATION

The model topography approximates the northern side of Georges Bank at about 42.1°N, 66.8°W, which is the location of

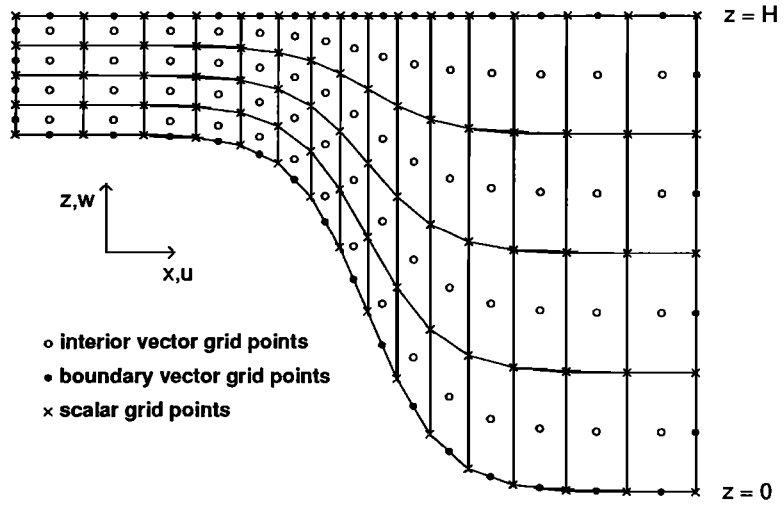

Fig. 1. A schematic of the computational grid showing the interior and boundary vector points (solid and open circles) and the scalar vector points (crosses). The horizontal stretching of the grid away from the bank edge is exaggerated.

the observations discussed by *Loder et al.* [1992] and *Brickman and Loder* [1993]. It is given by

$$z = h(x) = 97.5(1 - \tanh(dx)). \tag{6}$$

x and z are in meters. The water depth varies from 65 m on top of the bank to 260 m off the bank, with the latter being an idealization of the depths of up to 350 m found in Georges Basin. This has little influence on the results. Indeed, increasing the deep water depth to 320 m showed very little change in the model results (see section 5.2). The width parameter d has a value of 0.000225 m^{-1}, giving a steepest slope of -0.022. In order to investigate the influence of the slope of the topography some model runs were done by varying d so that the slope ranged between half and double this value. Figure 2 compares the actual topography taken along the observational cross section with the basic model topography given above and with the two extreme topographies used.

The model was initialized with a horizontally uniform density field. Observations show a substantial horizontal variation in the stratification, ranging from weakly stratified on top of the bank to strongly stratified off the bank [*Loder et al.*, 1992]. From the point of view of the wave generation the stratification of the fluid over the bank edge, where the waves are generated, is most relevant. This stratification varies with time due to tidal advection. A stratification based on tidally averaged observations close to the bank edge is the most appropriate for model studies with a horizontally uniform stratification.

Two density profiles have been used. The base density profile is a fit to the averaged density profile on top of the bank close to the edge at 42.130°N. It is given by

$$\rho_1 = \begin{cases} f(z) + 0.0000045(z-250)^2, & 250 \le z \le 260; \\ f(z), & \text{if } z < 250, \end{cases} \tag{7a}$$

where

$$f(z) = 0.02573 - 0.002\exp\left(\frac{z-260}{18}\right) + \frac{0.00017}{1+\left(\frac{z-240}{8.5}\right)^2} - \frac{0.00021}{1+\left(\frac{z-252}{9}\right)^2}. \tag{7b}$$

The second density profile is

$$\rho_2 = \begin{cases} 0.02453, & 250 \le z \le 260; \\ 0.02731 - 0.0033955\exp\left(\frac{z-260}{50}\right), & \text{if } z < 250 \end{cases} \tag{8}$$

This profile approximates the observed density profile just off the bank edge at 42.235°N.

In Figure 3, density profiles ρ_1 and ρ_2 are shown along with the observed density profiles which they approximate. Note that for $\rho_1(z)$ the data extend over the upper 65 m only. The density profile was arbitrarily chosen to approach a constant value of 0.02573 exponentially. As discussed in section 5, results obtained using $\rho_2(z)$ show that the effects of stratification at depth can be very significant. The dynamically significant difference between the two density profiles is illustrated by their buoyancy frequency profiles $N(z)$, which are shown in Figure 4. The differences in N result in changes in wave propagation speeds and in the slope of the paths followed by wave packets. The maximum value of the horizontal group velocity of vertically trapped waves is close to the linear long-wave, nonrotating phase speed, the values of which for mode one and two waves are plotted in Figure 5 as a function of water depth.

The final problem regarding the model initialization is to choose the initial velocity fields. Consider an inviscid, unstratified flow. If the forcing at the boundaries is sinusoidal and independent of z then u and v are very nearly independent of z throughout the domain. Assuming this, u is given by

$$u = \frac{Q}{r(x)}\sin(\omega t + \phi) \tag{9}$$

where Q is the maximum cross-bank volume flux, $r(x) = 260 - h(x)$ is the local fluid depth, and ω is the tidal frequency. Continuity gives

$$w = Q\frac{r'(x)}{r^2(x)}(z - 260)\sin(\omega t + \phi). \tag{10}$$

If the fluid depth was constant u would be independent of x. Assuming v was as well, with a tidal average of zero and zero along-bank pressure gradient, we have

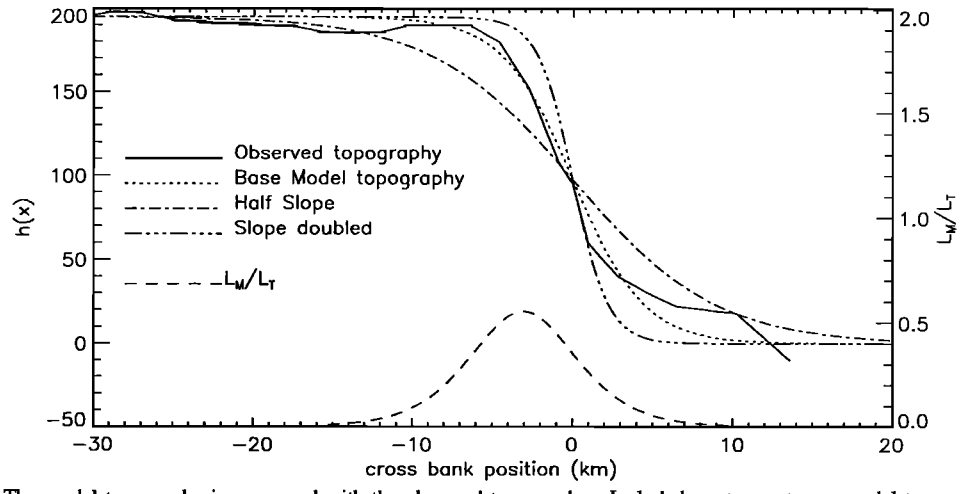

Fig. 2. The model topography is compared with the observed topography. Included are two extreme model topographies used, with the slope halved and doubled. Also plotted is the nonlinear parameter L_M/L_T, the ratio of the tidal excursion distance to the horizontal topographic length scale.

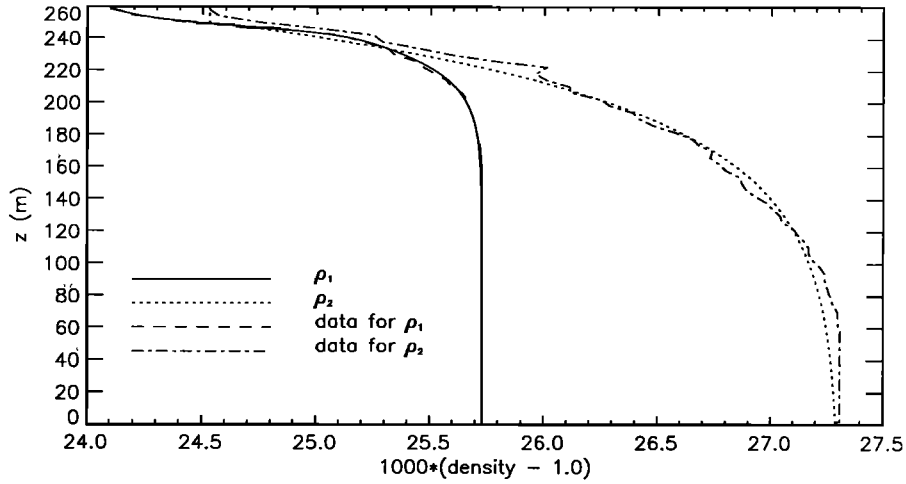

Fig. 3. The two density profiles used in model runs along with the observed density profiles which they approximate.

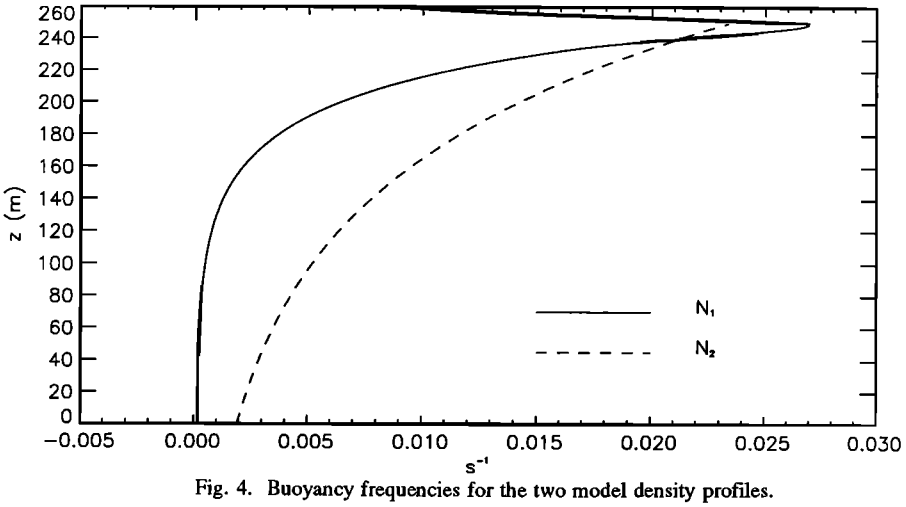

Fig. 4. Buoyancy frequencies for the two model density profiles.

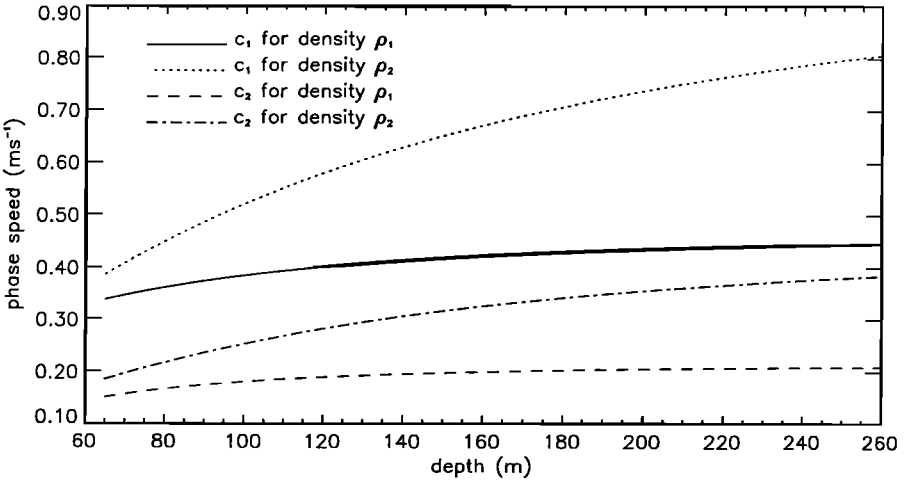

Fig. 5. Linear, nonrotating phase speeds in the long-wave limit as a function of water depth. These approximate the maximum group velocity in the rotating frame.

$$v = \frac{fQ}{\omega r}\cos(\omega t + \phi). \tag{11}$$

This yields clockwise tidal ellipses aligned in the cross-bank direction with ellipticity factor ω/f.

Following the above, the velocity fields are initialized via

$$u = \frac{Q}{r(x)}\sin(\phi)$$

$$v = \frac{fQ}{\omega r(x)}\cos(\phi) \tag{12}$$

$$w = Q\frac{r'(x)}{r^2(x)}(z-260)\sin(\phi)$$

The value of ω was chosen to give a 12.4-hour tidal period (τ), giving $\omega \approx 1.4075 \times 10^{-4}\ s^{-1} \approx 1.4f$. The base value of Q is 59.8 $m^2\ s^{-1}$, approximating observed values. Usually the phase ϕ was set to zero, so that the model runs start at the beginning of off-bank flow. While somewhat arbitrary, it can be justified on the basis that observations show that the isopycnals are relatively flat at the start of off-bank flow [*Brickman and Loder*, 1993]. Other values of Q and ϕ were used to test the sensitivity of the results.

The initialization (12) means that far from the bank edge v varies sinusoidally with a mean value of zero (prior to the arrival of any waves). Integrating equation (1*b*) over the computational domain and averaging shows that the nonlinear advective term results in a tidally averaged along-bank tidal Eulerian transport

$$\bar{E} = \frac{1}{4}\frac{fQ^2}{\omega^2}\left(\frac{1}{r_L} - \frac{1}{r_R}\right)(1 - 2\sin^2(\phi)). \tag{13}$$

The tidally averaged along-bank Lagrangian transport is

$$\bar{L} = \bar{E} + \frac{1}{2}\frac{fQ^2}{\omega^2}\left(\frac{1}{r_L} - \frac{1}{r_R}\right) \tag{14}$$

where r_L and r_R are the water depths at the left and right boundaries, respectively. The difference $\bar{L}$ - $\bar{E}$ is positive in this case and is consistent with previous results [e.g., *Loder*, 1980], which indicate that the Stokes transport depends only on the tidal ellipses and not on friction.

The nondimensional parameter L_M/L_T, where L_M is the tidal excursion distance

$$L_M = \frac{Q}{r(x)\omega}, \tag{15}$$

and L_T is the horizontal length scale

$$L_T = \frac{r(x)}{r'(x)}, \tag{16}$$

is an indicator of the nonlinearity of the problem. Its value for the base case run is plotted in Figure 2 with the topography. The location of its peak value (about 0.55 at $x \approx$ -3 km) is where the strongest forcing of the internal wave motion is expected [*Baines*, 1982].

The value of $\bar{E}$ is positive if $\phi = 0$, implying a mean along-bank jet in the positive y direction. Observations show the presence of an along-bank jet in the opposite direction. This jet arises from a number of related factors including the influence of friction on tidal rectification and the presence of a tidal front over the bank edge [*Loder*, 1980]. Because the physical processes which drive this along-bank jet are not present in the model, runs with more realistic along-bank flow will be left for future work when correct horizontal density structure and frictional effects will be included. The model results are not very sensitive to the initialization of v (section 5.5).

4. BASE CASE RUN: RESULTS AND DISCUSSION

The base case uses density profile ρ_1 and topography (6) with d = 0.000225. The velocity fields are initialized using (12) with $\phi = 0$ and $Q = 59.8\ m^2\ s^{-1}$. This results in a maximum horizontal velocity U_{max} of 0.92 m s^{-1} on top of the bank. Thus at $t = 0$ the density field is horizontally homogeneous and the fluid is starting to move off-bank from its maximum on-bank position. Contour plots of the density field every eighth of a tidal period during the first two periods are shown in Figure 6. For this run the grid resolution is 40 evenly spaced grid points in the vertical, giving 1.625 m and 6.5 m vertical resolution in the shallow and deep water, respectively. The horizontal resolution ranges from 74 m at x = ±30 km to 20 m over the bank edge. Some of the sensitivity runs had half this horizontal resolution. The computational domain extends between x = ±64 km. No waves reached either boundary during the model runs.

In sections 4.1 and 4.2, an overview of the first and second tidal period depicted in Figure 6 is presented. The results of the base case run are discussed in more detail in section 4.3.

4.1. First Tidal Period

During the off-bank flow, the net volume flux into the computational domain below any isopycnal is negative (except for the isopycnal at the surface) since, below a given isopycnal, more fluid leaves the domain at the right boundary (at $x \approx$ 64 km) than enters at the left boundary (at $x \approx$ -64 km) because of the vertically uniform velocities at these boundaries. Hence during the early stages of off-bank flow a depression forms over the bank edge. From this depression two depressions are generated, one propagating in either direction. This is first apparent at t = 0.25 τ (although they have not yet completely separated). After t = 0.375 τ the on-bank and off-bank propagating waves are clearly identifiable (labelled A_1 and C_1, respectively, in Figure 6). The off-bank propagating wave is advected away from the bank and hence has little chance to grow in amplitude through the superposition of waves which are continually being generated.

The on-bank propagating depression A_1 propagates against the flow and hence moves much more slowly away from the generation region. The flow on top of the bank quickly becomes supercritical, so that depression A_1 is trapped, resulting in a large, narrow wave. The faster flow and slower group velocities in the shallow water on top of the bank both act to strengthen the asymmetry between the on and off-bank propagating depressions (and weaken it when the flow is on-bank). Table 1 gives the mode-n Froude numbers Fr_n at various times of the tidal period for the first two modes in the deep and shallow water. Fr_n is defined as the ratio of the flow speed (vertically averaged) to the maximum horizontal group velocity for a mode-n wave using the undisturbed density profile. The maximum group velocity is approximated by the linear nonrotating long-wave phase speed with a small error (see section 4.3). Table 1 shows that the shallow water flow becomes supercritical ($Fr > 1$) to mode 1 waves sometime between $t = \tau/32$ and $t = \tau/16$, where τ is the tidal period. Thus, in all of the contour plots in Figure 6 the off-bank flow on top of the bank is supercritical to all waves. In contrast, the deep-water flow is subcritical to mode-one waves throughout the tidal period, and is barely supercritical to mode-two waves at peak flow. Table 1 gives the critical water depths where the Froude number is equal to 1 for various shallow-water speeds. Waves cannot propagate against the flow into shallower water and hence are arrested at locations with these depths. The values in the table were computed assuming that the density profile at a position x is the same as the original and that the horizontal velocity is vertically uniform. Because the fluid is vertically stretched as it moves off-bank, weaker stratification and lower linear phase speeds would be expected. Thus, the true critical depths are slightly deeper (barring shear effects). At t = 0.375 τ the flow speed on top of the bank is about 0.65 ms^{-1} and the

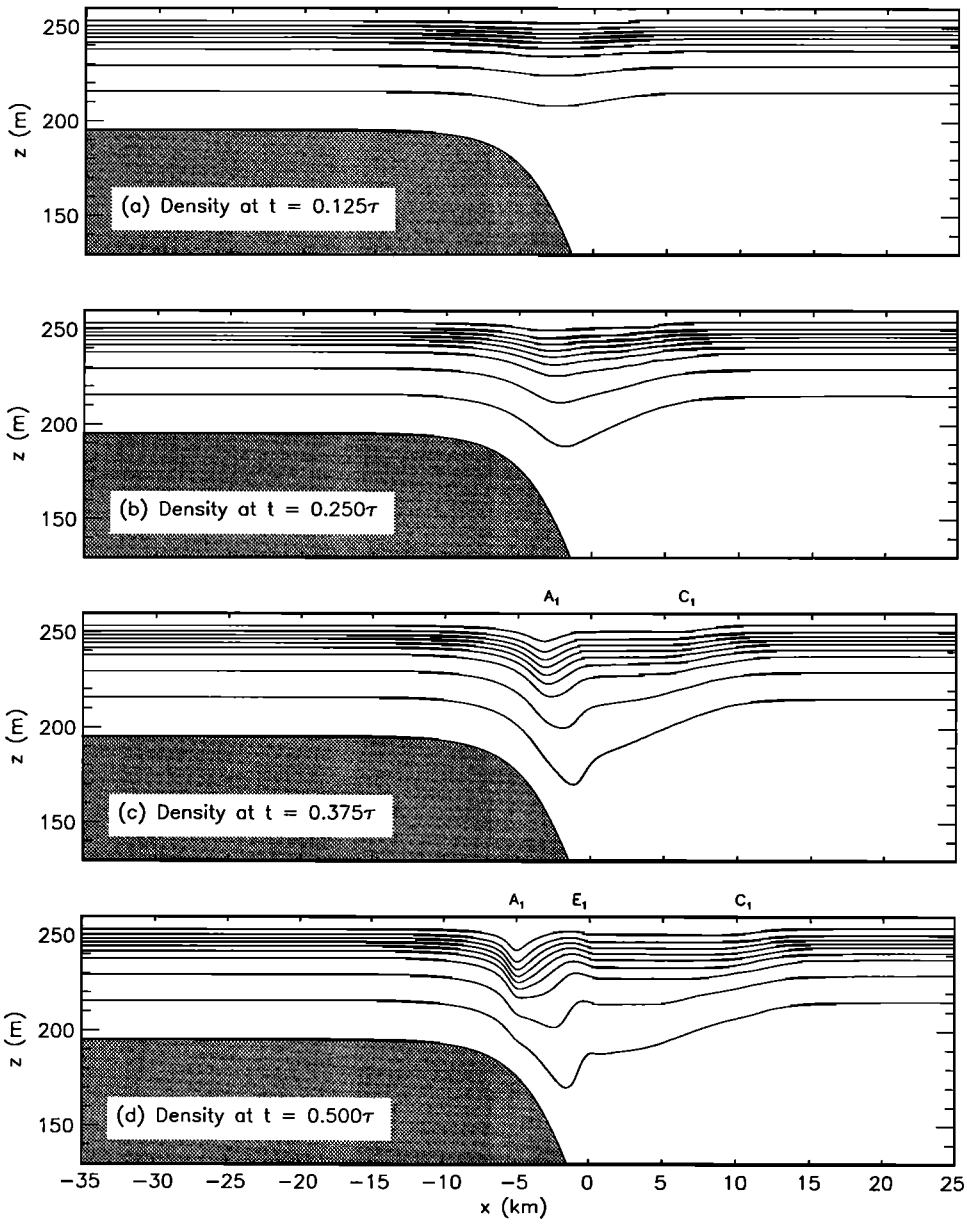

Fig. 6. Contour plots of the density fields for the base case. Only part of the computational domain is shown. See text for discussion of labeled features.

critical depth is about 108 m (at about x = -2.8 km). Figure 6*c* shows the on-bank propagating wave at approximately this location (see also Figure 11). During the on-bank portion of the tidal period, the leading edge of the depression steepens due to nonlinearities.

At t = 0.5 τ the off-bank flow has ended and an upward bulge in the isopycnals can clearly be seen developing slightly to the left of the center of the bank edge (Figure 6*d*). Its growth is coupled with downwelling and a further deepening of depression A_1 over the bank edge. Vertical velocities have peak values of about -0.57 and 0.48 cm s^{-1} in the downwelling and upwelling regions. The elevation tilts up to the left (Figures 6*d* and 6*e*). Between t = 0.5 τ and 0.625 τ, it grows. It then broadens as it is advected onto the bank (Figures 6*e*-6*h*). Concurrently, it splits into two elevations, one propagating in either direction. Trailing the on-bank propagating elevation (E_1) is an on-bank propagating, near surface depression (labelled B_1) below which the isopycnals are displaced upward. By t = 0.875 τ, E_1 is clearly a mode-one wave. Following it, the surface depression B_1 is now clearly a mode-two wave. Whether this distinction can be made at an earlier stage is unclear, as the changes in the vertical structure are affected by vertical shear. E_1 and B_1 gradually separate.

As the on-bank flow increases, a broad elevation of the isopycnals develops over the bank edge (F_1). It is largely due to the upwelling associated with the on-bank flow but includes the off-bank propagating wave mentioned above.

4.2. *Second Tidal Period*

The second tidal period can be regarded as a sensitivity study, with the initial conditions given by the velocity and density fields at t = τ. The most relevant feature is the elevated isopycnals F_1 centered at about x = -5 km (Figure 6*h*) and the associated velocity fields (Figure 7). Depressions A_1 and C_1 are too far from the bank edge to play a role in the second tidal period. The mode-two wave B_1 is advected back over the bank edge and

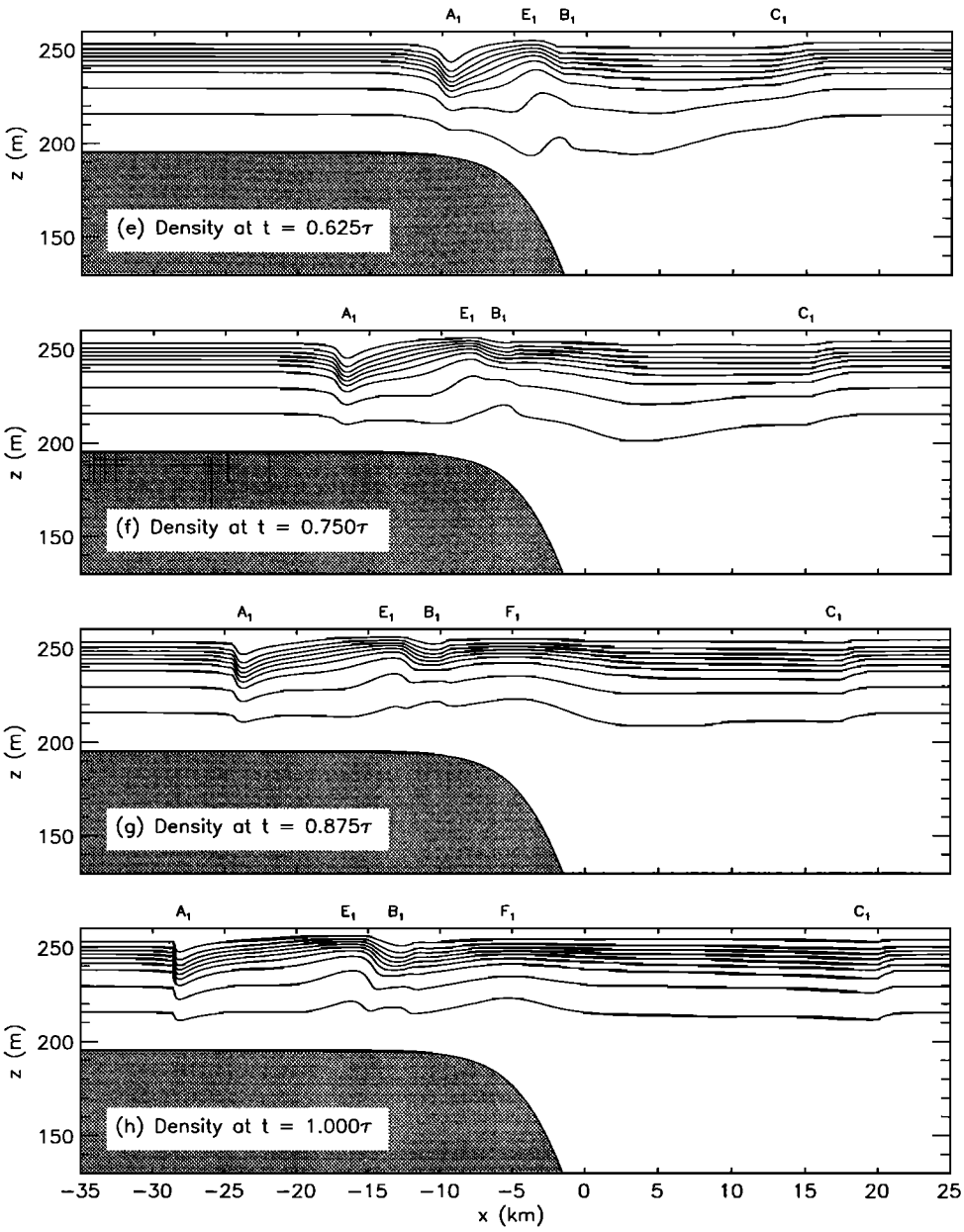

Fig. 6. (continued)

presumably influences the wave generation during the second tidal period. The horizontal and vertical velocity fields show the presence of a vortex of negative vorticity $\varsigma = u_z - w_x$ (i.e., anticlockwise rotation around the negative y axis) on the off-bank side of F_1. A vortex of opposite sign on the other side of the elevation overlaps the vortex associated with features E_1 and B_1.

In the center of elevation F_1, w has a minimum of about -0.1 cm s^{-1} at approximately middepth; w is over twice as large farther off-bank at the bottom, where it goes as low as -0.26 cm s^{-1}. For comparison, the minimum value of the vertical velocity associated with the barotropic flow, the flow in the absence of stratification, during peak off-bank flow is about -0.90 cm s^{-1}. It occurs in about the same location, which is farther off-bank than the location of the maximum of L_M/L_T (see Figure 2). The maximum value in the upwelling region off the bank is about 0.1 cm s^{-1} 60 m below the surface. The downwelling associated with depression B_1 has a minimum of about -0.27 cm s^{-1}. Over the bank edge, u ranges from -0.29 m s^{-1} at the surface to 0.17 m s^{-1} at the bottom. Thus, the baroclinic velocities are a significant fraction of the peak barotropic velocities.

The negative vortex plays a key role in the evolving wave field because its presence results in a much stronger response in the second tidal period. This is clearly indicated by the results of a model run with no tidal forcing initialized with the flow state of the base case run at $t = \tau$. An elevation propagates away from the bank, and a large depression develops over the bank edge. The depression attains a maximum size of about one third that of the depression seen in the base case run at $t = 0.5\ \tau$. In the upwelling region further off-bank the isopycnals rise by about 15 m at $x \approx 5$ km. There is not a corresponding rise on the on-bank side of the depression.

During the second tidal period the sequence of events seen in the first tidal period is repeated. The depression formed over the bank edge during the off-bank flow is approximately twice as deep as that formed during the first tidal period, because of the strong downwelling over the bank edge at the start of the second tidal

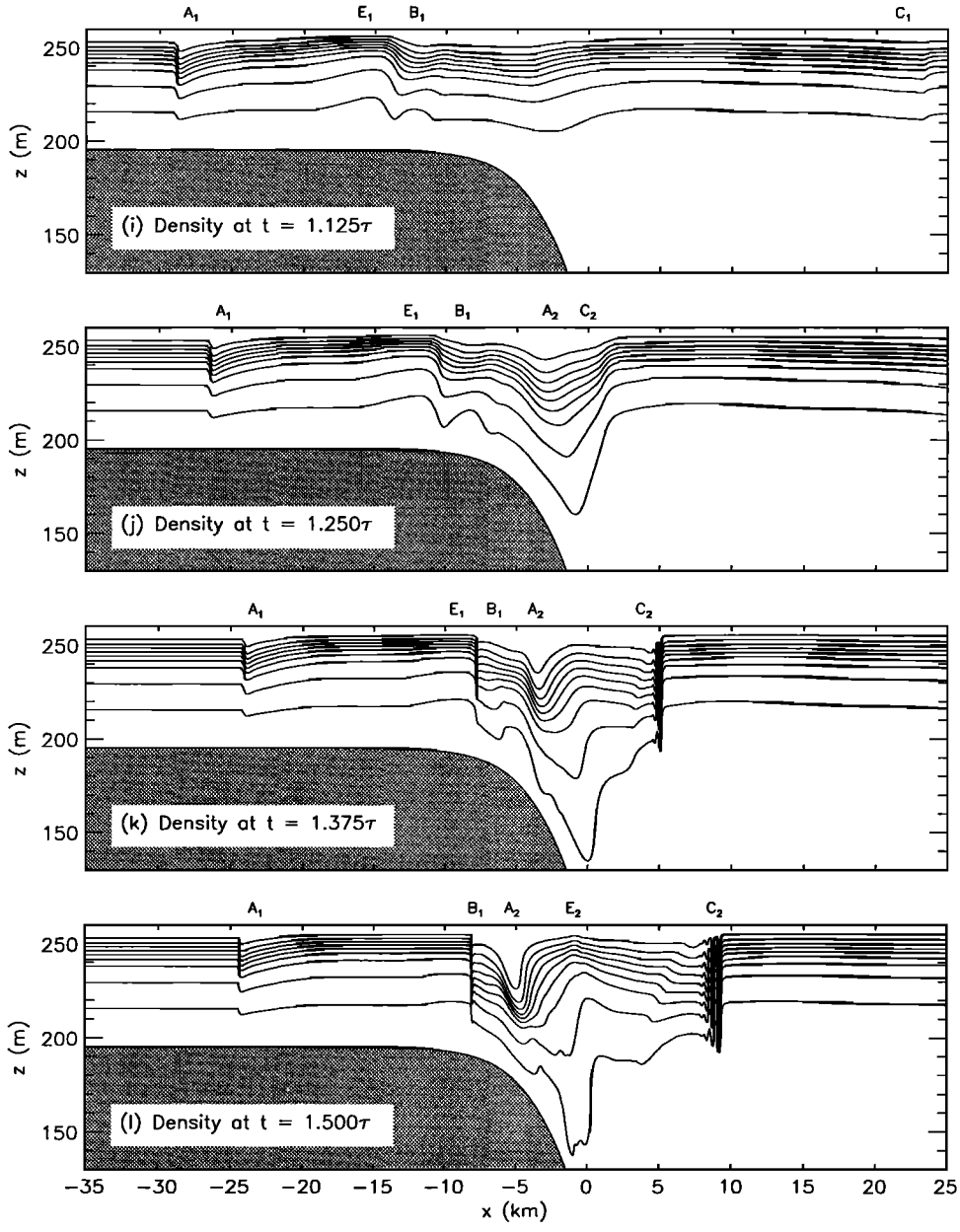

Fig. 6. (continued)

period. Conservation of volume implies that this must be accompanied by a raising of the isopycnals relative to their displacement one period earlier. This occurs farther off-bank. For example, in Figure 6*b* the isopycnals are depressed out as far as x = 5 km, whereas one period later (Figure 6*j*) the depression extended only to about 2 km. The isopycnals are in fact above their rest position between about 2 and 15 km in the latter case, with a peak rise of about 6 m at x = 7 km. The larger depression formed over the bank edge results in larger, steeper depressions (labelled A_2 and C_2) propagating onto and away from the bank.

As in the first tidal period, a sudden rise of the isopycnals occurs almost halfway into the tidal period at $x \approx 0$ (Figures 6*k* and 6*l*). This is again coupled with downwelling. The result is the formation of very steep isopycnals near the bottom over the bank edge. The upward sloping isopycnals are referred to as a hydraulic jump. This is the location where overturning first occurs. Overturning has occurred in this case deeper down in a very weakly stratified region at the bottom between depths of about 140 and 200 m centered at x = 3 km. It appears to be a result of a shear instability. At t = 1.25 τ the Richardson number, $Ri = -g\rho_z/u_z^2$, is less than 0.25 in a region approximately 4 km long at the bottom centered at $x \approx$ -0.5 km. Minimum values of Ri are about 0.07. In the numerical model nothing special is done to handle the overturning. When overturning occurs, the fluid is locally unstable. The developing instability results in rising and falling fingers of fluid. These result in the high-frequency short waves with horizontal wavelengths of O(300 m) first seen at t = 1.625 τ between x = 0 and 3 km. These short waves are well resolved in the model.

During the off-bank flow phase of the second tidal period, elevation E_1 and the mode-two wave B_1 continue to separate while being advected back to the bank edge. The latter disappears into the large depression formed over the bank edge. Between E_1 and B_1, a mode-one depression forms. This also occurs in the model run with the tidal forcing turned off after the first tidal period. The mode-one depression (to which B_1 now refers) is barely

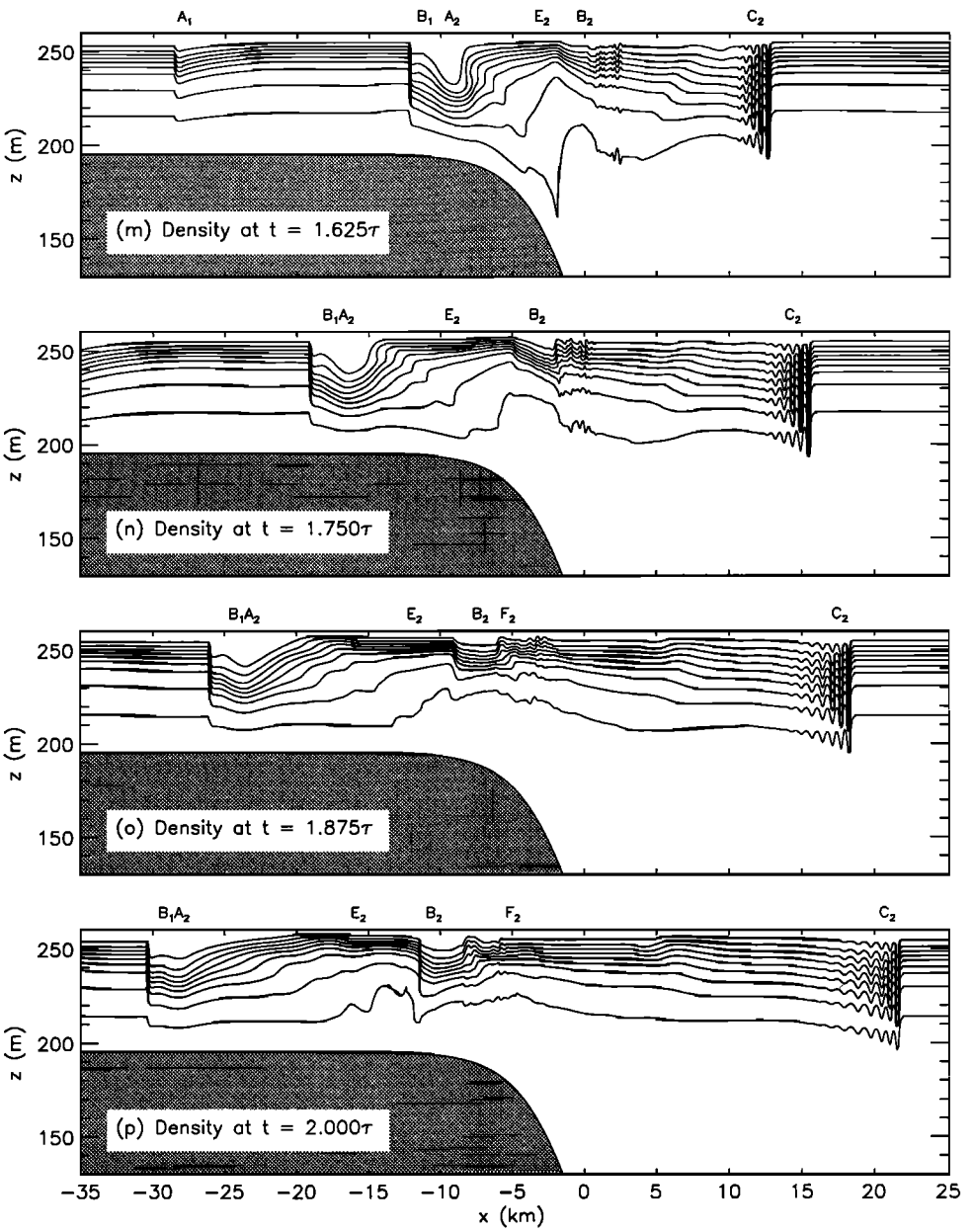

Fig. 6. (continued)

TABLE 1. Froude Numbers and Critical Depths

Time	U (Shallow)	Fr_1 (Shallow)	Fr_2 (Shallow)	U (Deep)	Fr_1 (Deep)	Fr_2 (Deep)	Mode 1 Critical Depth	Mode 2 Critical Depth
1/32 τ	0.179	0.532	1.193	0.045	0.100	0.214	___	73
1/16 τ	0.352	1.043	2.340	0.088	0.197	0.420	67	121
3/32 τ	0.511	1.514	3.397	0.128	0.286	0.609	89	166
1/8 τ	0.651	1.927	4.324	0.163	0.364	0.776	108	206
5/32 τ	0.765	2.266	5.085	0.191	0.428	0.912	124	239
3/16 τ	0.850	2.518	5.650	0.212	0.475	1.013	135	___
7/32 τ	0.902	2.673	5.998	0.226	0.505	1.076	142	___
1/4 τ	0.920	2.726	6.115	0.230	0.514	1.097	144	___

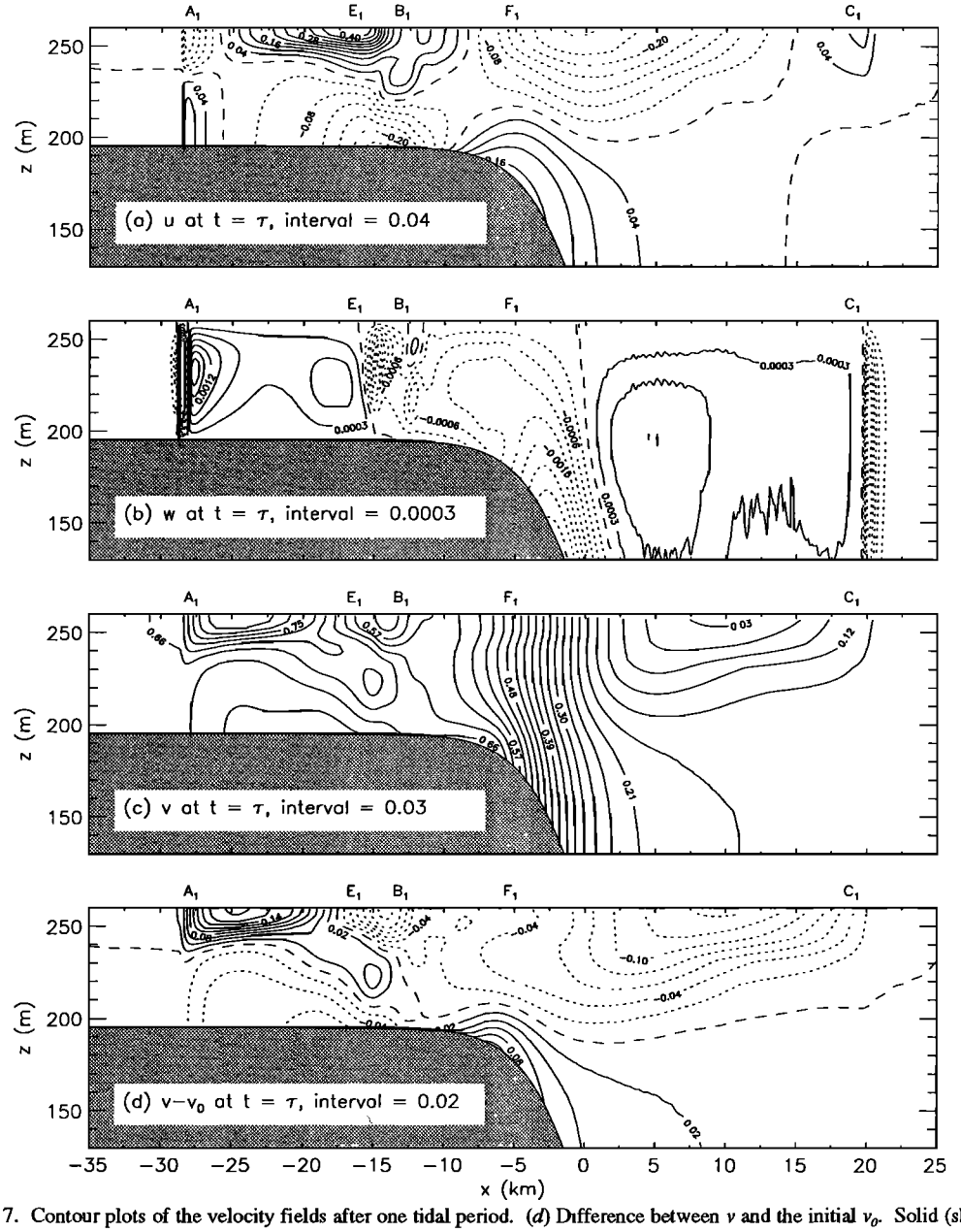

Fig. 7. Contour plots of the velocity fields after one tidal period. (*d*) Difference between v and the initial v_0. Solid (short dashed) lines are positive (negative) values. The long dashed lines are the zero contours. The minimums of w associated with depressions A_1 and C_1 are -0.015 m s^{-1} and -0.0018 m s^{-1}, respectively.

distinguishable from the initial on-bank propagating depression (A_2) formed during the second tidal period. The two combined form a long depression B_1A_2. At its tail end there is some overturning. After two tidal periods, B_1A_2 has a sharp leading front which is about 1.5 km farther from the bank edge than depression A_1 was a period earlier (the A_2 part of the depression is at the same location). Depression B_1A_2 with jumps at both ends of it is similar to the large depressions with leading and trailing jumps observed by *Holloway* [1987] in shallow water on the Australian North West Shelf, although the generating mechanism may be different. In Holloway's observations the trailing jump showed no signs of overturning and a single depression was believed to have been generated far away in deeper water. *Smyth and Holloway* [1988] explained the jumps in front and behind the shoreward propagating depressions as being due to second-order nonlinear processes which become important as the depression enters shallower water. This nonlinear mechanism could also explain this aspect of the numerical results.

At the end of the second on-bank flow stage a broad region (about 10 km long) of flat, slightly elevated near surface isopycnals (E_2) trails depression A_2. Following it, a sharp depression (B_2) is seen in the upper half of the water column. It is much more pronounced than the corresponding feature (B_1) formed in the first tidal period, and its leading edge is very steep. Depression B_2 is first noticeable at t = 1.625 τ, one period after the first appearance of depression B_1. A mode-two structure is evident, but not as apparent at $t = 2\tau$. Since a mode-two wave has larger isopycnal displacements near the bottom where the stratification is weakest, it appears that B_2 is the combination of a large mode-one depression and a small mode-two wave. A period earlier, B_1 was a more even mixture of these two types of waves. Depression B_2 lags depression B_1 a tidal period earlier by about 5

km, indicating some variability in the location of the second depression.

The off-bank propagating depression C_2 formed during the second tidal period is large enough for nonlinearities to steepen it, after which it disperses into an undular bore, as predicted by solutions of nonlinear equations of the KdV type [e.g., *Fornberg and Whitham*, 1977]. Space shuttle photographs of the Gulf of Maine show a group of four to six internal waves consistent with an undular bore, propagating away from the edge of Georges Bank once every tidal period [*Violette et al.*, 1990].

At the end of the second tidal period there is a broad elevation of the isopycnals, similar in strength to the corresponding feature seen after one tidal period. The model run was continued into the third tidal period. Early in the off-bank flow the steep front at the leading (on-bank) edge of depression B_2 overturned. The result was very high velocities and considerable mixing in the depression formed over the bank edge. The ensuing large velocities and small-scale features necessitated the termination of the model run. This indicates that the response after two tidal periods is not quasi-periodic.

4.3. Discussion of the Base Case Results

While the interaction with the waves generated in the first tidal period results in a significantly stronger response in the second tidal period, the essential features are the same. In both tidal periods the appearance of the second on-bank propagating depression just as the tide turns on-bank is in agreement with the observations [*Loder et al.*, 1992; *Brickman and Loder*, 1993], in which the first on-bank propagating depression A_n was seen every tidal period and the second was seen in 19 of the 26 tidal periods analyzed, or 73% of the time. In the real physical situation there are many factors which complicate the evolution of the flow field, such as strong mixing and the horizontally varying stratification. Variations in the phase of the tide with depth would also effect the evolving wave field. Wave dissipation could do two things. First, it could weaken the response in the second tidal period, giving a result somewhere in between the two seen here. In addition, the second of the two on-bank propagating depressions could dissipate due to the strong turbulent mixing on top of the bank and the mixing resulting from its propagation into a more weakly stratified region. Thus, it would no longer exist to get advected back over the bank edge.

In the following the first tidal period is used for a more detailed examination. The reasons for using the first tidal period are twofold. First, the basic internal wave generation mechanisms are clearest in the first tidal period, as interactions with waves generated in earlier tidal periods are absent. Second, for comparisons with observations the initial density field is closest to the observed state (i.e., relatively flat isopycnals over the bank edge), there is no influence from depressions generated in previous tidal periods (as appears to be the case in the observations) and also the vortex over the bank edge would presumably be weakened by frictional and turbulent effects. Thus, the interactions between different tidal periods is minimized. Any close quantitative agreement may be a result of this, but may also be fortuitous.

1. Significance of dispersion. Many features of the results, including the two on-bank propagating depressions, are a result of long-wave dispersion on a rotating f plane. For a constant depth r the vertical structure $\phi(z)$ of the vertical velocity of long waves is determined by the eigenvalue problem

$$\phi'' + \frac{N^2(z)}{\alpha}\phi = 0, \tag{17a}$$

$$\phi(0) = \phi(r) = 0. \tag{17b}$$

In terms of the eigenvalue α, the dispersion relation is

$$\sigma = \pm(f^2 + k^2\alpha)^{1/2} \tag{18}$$

where σ and k are the frequency and horizontal wave number of the wave. The phase and group velocities c and c_g are given by

$$c = \pm\left(\alpha + \left(\frac{f}{k}\right)^2\right)^{1/2}$$
$$c_g = \frac{\alpha}{c} \tag{19}$$

For density ρ_1, the first two eigenvalues are $\alpha_1 = 0.1156$ and $\alpha_2 = 0.0225$ in the shallow water and $\alpha_1 = 0.1999$ and $\alpha_2 = 0.0440$ in the deep water. Dispersive effects are significant only if f/k is similar in size to $\alpha^{1/2}$, i.e., if the horizontal wavelength is comparable to the internal Rossby radius $\alpha_1^{1/2}/f$, which is 3.4 and 4.5 km in the shallow and deep water, respectively. Since the width of the initial depression is about 10-15 km, dispersive effects are an important factor in the evolution of the wave field. Figure 8 compares the nonhydrostatic rotating and nonrotating phase speeds for small k. Also shown is the group velocity for the rotating case. Note that for the mode-one wave in deep water, either rotational effects or nonhydrostatic effects are important except possibly in a narrow region around $k \approx 0.002$ m^{-1}.

To illustrate the importance of dispersion, the numerical model was used to calculate the adjustment of an initial state consisting of a depression of the isopycnals with all the velocity fields set to zero. The depression was initially about 10 km wide with an amplitude of 30 m in water 130 m deep. Figure 9 shows the initial state along with the result after one tidal period for the nonrotating case. The adjustment is hydrostatic with two depressions (labelled A and C) propagating away in either direction. Significant nonlinear steepening is apparent. Trailing each depression by about 15 km is a mode-two wave. In Figure 10 the adjustment of the same initial depression is shown for the rotating case ($f = 10^{-4}$). The two leading depressions A and C propagating away from the center are followed by a second pair of depressions (labelled B and D) separated by an elevation approximately 10 km long.

In the case of tidal flow across a bank edge the depression formed during the off-bank flow undergoes a similar adjustment. This can be seen most clearly by considering the difference between the base case run and a repetition of it with the gravitational term g set to zero. Setting $g = 0$ is equivalent to using an unstratified fluid, with the isopycnals now being thought of as material curves. It gives the barotropic flow. When this is done, a strong depression develops over the bank edge during the off-bank phase of the tidal period. This depression is much larger than in the nonzero g case because internal waves can no longer propagate away from the bank edge. It reaches a maximum size after half a tidal period and diminishes after the tide turns. After a complete tidal period, the isopycnals are essentially flat, and the flow state is almost identical to the state at $t = 0$ (no differences in the contour plots can be seen). This is expected, since for an unstratified, constant-depth fluid on an f plane, the dispersion relation is

$$\sigma = \frac{fm}{(k^2+m^2)^{1/2}} \tag{20}$$

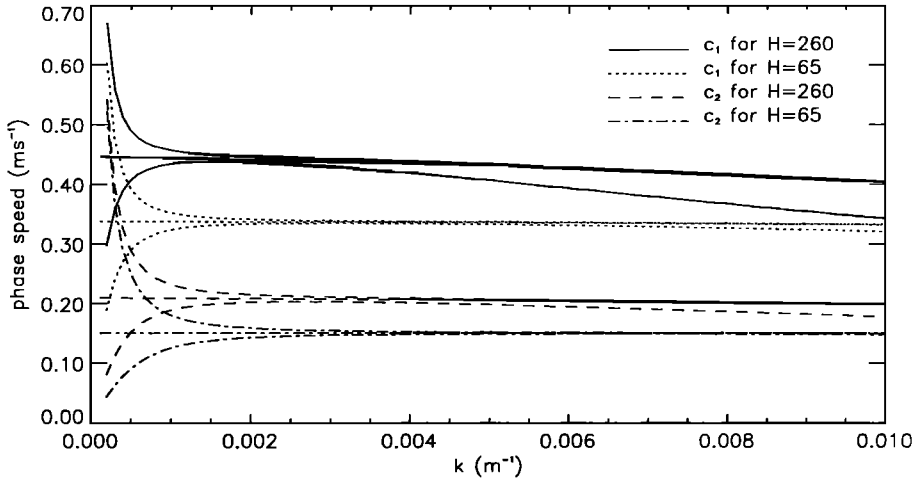

Fig. 8. Nonhydrostatic propagation speeds for mode-one and mode-two waves for density ρ_1 in depths of 65 and 260 m as a function of the horizontal wave number k. The three curves for each case are, from top to bottom, the rotating phase speed, the nonrotating phase speed, and the rotating group velocity.

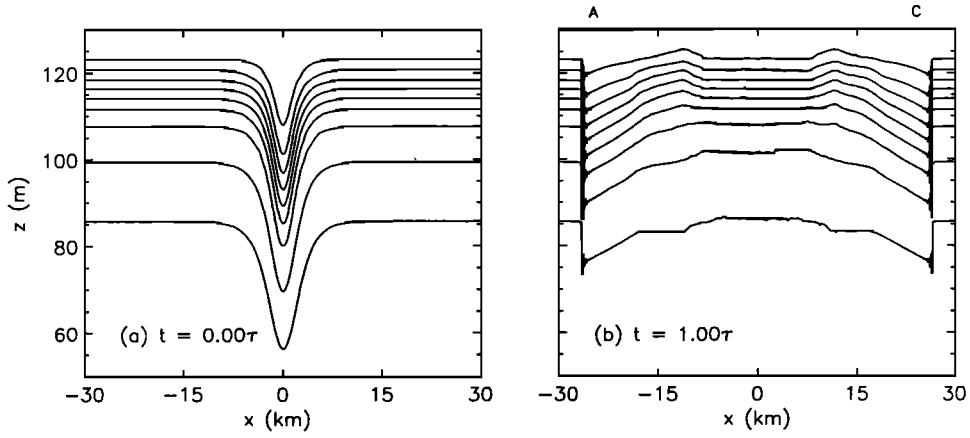

Fig. 9. The evolution of an initial rest state in a nonrotating frame. (*a*) The initial state and (*b*) the state one tidal period later (44640 s). Two mode-one depressions propagate away from the initial depression. Mode-two waves follow. In the center the isopycnals relax to their undisturbed position.

where k and m are the horizontal and vertical wave numbers. Only waves with a frequency less than f can occur. Since the frequency of the forcing is about 1.4 f, none of these waves are significantly excited after one tidal period. Furthermore, the maximum propagation distance of these waves is about $8/n$ and $32/n$ meters in one tidal period for a mode n wave in the shallow and deep water, respectively. The net result is the negligible isopycnal displacements after one tidal period.

The solution for $g = 0$ is now subtracted from the original solution. The difference in the density fields $\delta\rho(x,z,t)$ is vertically integrated to find the potential energy anomaly

$$pe(x,t) = 9.8 \int_{h(x)}^{260} \delta\rho(x,z,t) z\, dz \qquad (21)$$

due to the waves. Plots of pe as a function of x are given at various times in Figure 11. The picture that emerges from these plots is the following.

Immediately after the depression over the bank edge is formed at the start of the off-bank flow, gravitational restoring forces in the nonzero g case result in an upward movement of the center of the depression relative to the $g = 0$ case. This is apparent as early as $t = 0.125\ \tau$, as indicated by the positive pe. Meanwhile two depressions propagate away, one in either direction. The peak in pe centered at about $x = 0$ reaches its maximum between about 0.5 τ and 0.625 τ. Thereafter it collapses to about one sixth of its peak value by $t = \tau$ and two elevations start propagating away, one in either direction. This is further evidence that part of the elevation F_1 seen over the bank edge at $t = \tau$ is partially comprised of an off-bank propagating wave generated by the continual dispersive adjustment of the initial depression formed during the off-bank flow. Note that during the on-bank flow, the off-bank propagating wave is propagating against the current and hence does not travel very far. Parts of it are in fact advected back onto the bank.

In Figure 12, results of a model run for which the tidal forcing was turned off at $t = 0.5\ \tau$ (the end of off-bank flow) are shown. Two depressions (A_1,B_1) separated by an elevation (E_1) can be seen propagating onto the bank. A mode-two wave partially superimposed on the second depression can be seen. This shows that on-bank flow is not responsible for the generation of these features.

2. Propagation speeds. Estimates of the wave propagation speeds relative to the vertically averaged flow are computed in the following manner. First the horizontal change in position Δx of a wave crest or trough (or of an isopycnal displacement of a

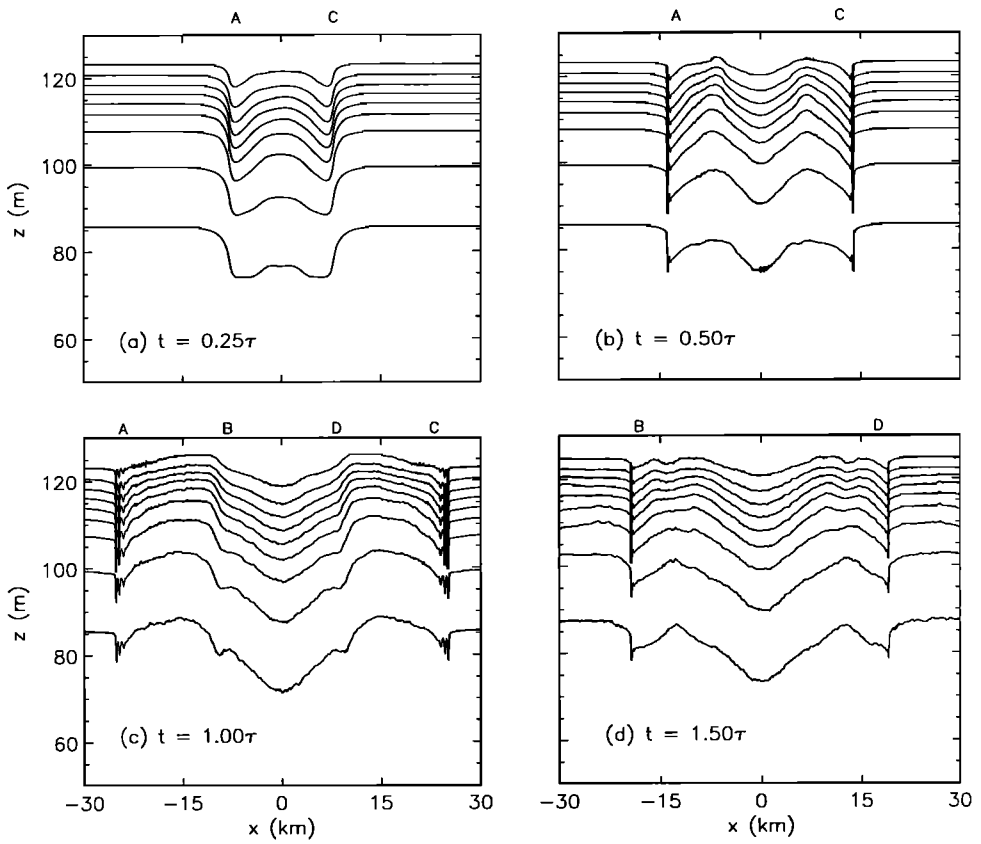

Fig. 10. The evolution of an initial rest state in a rotating frame ($f = 10^{-4}$ s^{-1}). The initial state is shown in Figure 9*a*. Long-wave dispersion gives rise to the elevated isopycnals and second depressions (*B* and *D*) seen propagating behind the initial depressions (*A* and *C*).

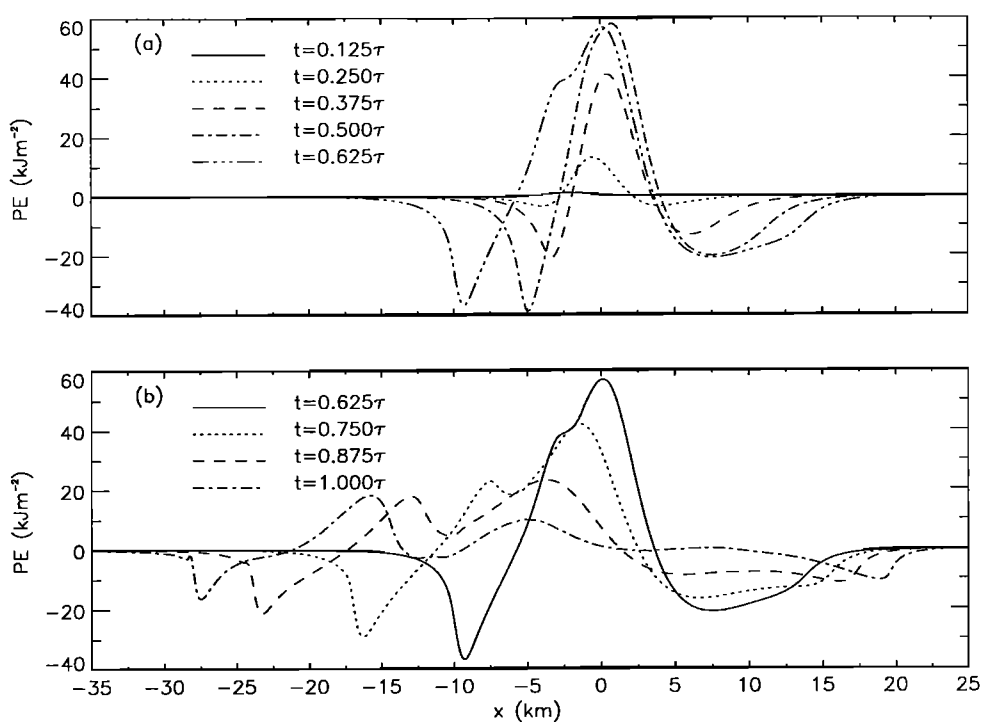

Fig. 11. The difference between the vertically integrated potential energy of the base case and that for the corresponding case with $g = 0$ is plotted as a function of x every eighth of a tidal period for the first tidal cycle.

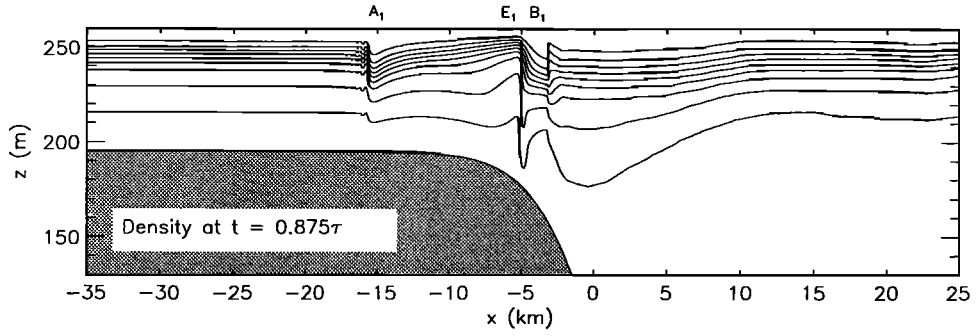

Fig. 12. Contour plot of the density field at $t = 0.875\ \tau$ for the base case but with the tidal forcing switched off at the end of the off-bank flow ($t = 0.5\ \tau$).

specified amount) between times t_1 and $t_1 + \delta t$ is measured. The contribution to the displacement by the vertically averaged flow $u(x,t)$ is computed using

$$\frac{dx}{dt} = \bar{u} = \frac{Q}{H-h(x)}\sin(\omega t+\phi). \tag{22}$$

This is easily integrated using (6) to give

$$F(x,t) = 162.5x + \frac{97.5}{d}\ln(\cosh(dx)) + \frac{Q}{\omega}\cos(\omega t+\phi) = const. \tag{23}$$

Thus the change in position δx in time δt of a wave which was at position x_1 at time t_1 due to advection by the vertically averaged flow is given by solving

$$F(x_1+\delta x, t_1+\delta t) = F(x_1,t_1).$$

The propagation speed of the wave relative to the water is then given by

$$c = \frac{\Delta x-\delta x}{\delta t}.$$

At the end of the first tidal period, depression A_1 has a maximum isopycnal displacement of about 5 m. Its propagation speed, relative to the barotropic flow, is about -0.40 m s^{-1}. The minimum of the depression propagates somewhat faster, at about -0.45 m s^{-1}, due to nonlinearities. For comparison, the nonrotating long-wave linear phase speed is about 0.34 m s^{-1}. It is well known that nonlinearities can increase propagation speeds by this amount (see *Gear and Grimshaw* [1983] or *Sandstrom and Elliott* [1984] for specific examples).

The broad elevation propagating onto the bank behind depression A_1 has a maximum isopycnal displacement of about 8 m at middepth. Estimating its propagation speed is difficult. Its peak displacement occurs at its tail-end, where it appears to have a mode-two structure. Indeed the peak and depression B_1 are propagating with a speed of about -0.17 m s^{-1}, close to the mode-two phase speed of about -0.15 m s^{-1}. The forward portion of the wave is propagating much more rapidly, with estimates ranging from about -0.34 m s^{-1} for the part of the wave just in front of the peak to about -0.45 m s^{-1} as depression A_1 is approached. The elevation of the isopycnals over the bank edge is continually being modified due to upwelling during the on-bank flow, so it is meaningless to discuss its phase speed.

Finally, well off the bank a weak depression C_1 is propagating away from the bank edge at about 0.44 m s^{-1}, in good agreement with the linear phase speed of about 0.447 m s^{-1}. The bottom of the depression is moving considerably faster at about 0.64 m s^{-1}, indicating that the wave is steepening due to nonlinearities.

At the end of the second tidal period, depression B_1, now taken as the mode-one depression which has separated from the mode-two wave, is propagating at about -0.43 m s^{-1}, similar to the speed of the mode-one depression A_1 a period earlier. Immediately following is depression A_2 propagating at about -0.48 m s^{-1}. The propagation speed of depression B_2 is about -0.14 m s^{-1}, indicating it is a mode-two wave at this time. The large undular bore, in the deep water (C_2) has a propagation speed of about 0.69 m s^{-1}.

3. Potential and kinetic energies. The energy associated with the depressions propagating away from the generation region is of considerable interest. The vertically integrated available potential energy (*APE*), is computed using the linear approximation [*Gill*, 1982]

$$APE = \frac{1}{2}\int_{h(x)}^{260}\left(\frac{g^2\rho'^2}{N^2}\right)dz. \tag{24}$$

ρ' is the perturbation from the reference state and N is the buoyancy frequency of the reference state. In this case the reference state is the initial density field. Hence this formula is used only at $t = \tau$ and $t = 2\tau$.

Figure 13*a* shows *APE* as a function of x for $t = \tau$ and $t = 2\tau$. In Figure 13*b* the cumulative horizontal integration of *APE* from the left boundary

$$\int_{x_1}^{x} APE\ dx,$$

is plotted. The latter plot is used to determine the total energy (per unit length along the bank) in a feature lying between x_1 and x_2 by taking the difference in values at the two end points. After one period depression A_1, at $x \approx -28$ km, contains about 2.5 MJ m^{-1} of available potential energy. *Brickman and Loder* [1993] estimate the first on-bank propagating depression seen in the observations to be about 2 km wide with an average available potential energy of 23 J m^{-3} over a 60 m depth, giving a total energy of 2.8 MJ m^{-1}. This compares well with the model result after one tidal period. The total available potential energy in depression B_1 is considerably smaller, being slightly less than 1 MJ m^{-1}. This is also in reasonable agreement with the observations in which the second depression was estimated to have about half the *APE* of the first. The elevation between depressions A_1 and B_1 has about 4 MJ m^{-1}. Depression C_1 contains about 1 MJ m^{-1}.

The larger response in the second period is evident in the much larger energy values. After two tidal periods the model results

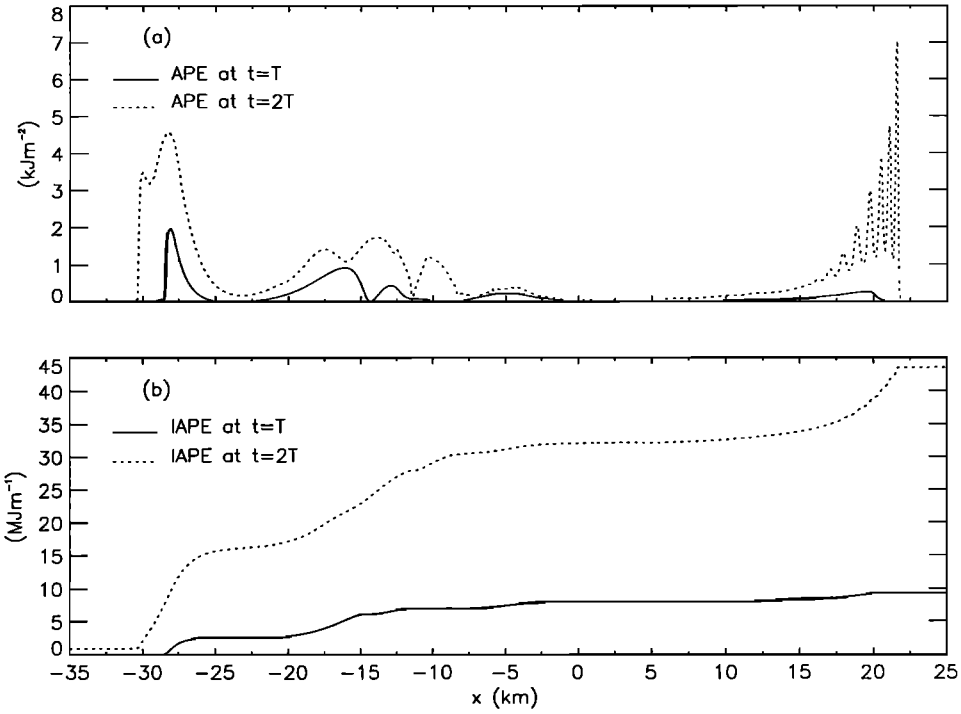

Fig. 13. Available potential energy. (*a*) Vertically integrated available potential energy *APE* after the first and second tidal period as a function of *x*. (*b*) Horizontal integral of *APE*, integrating from the left boundary.

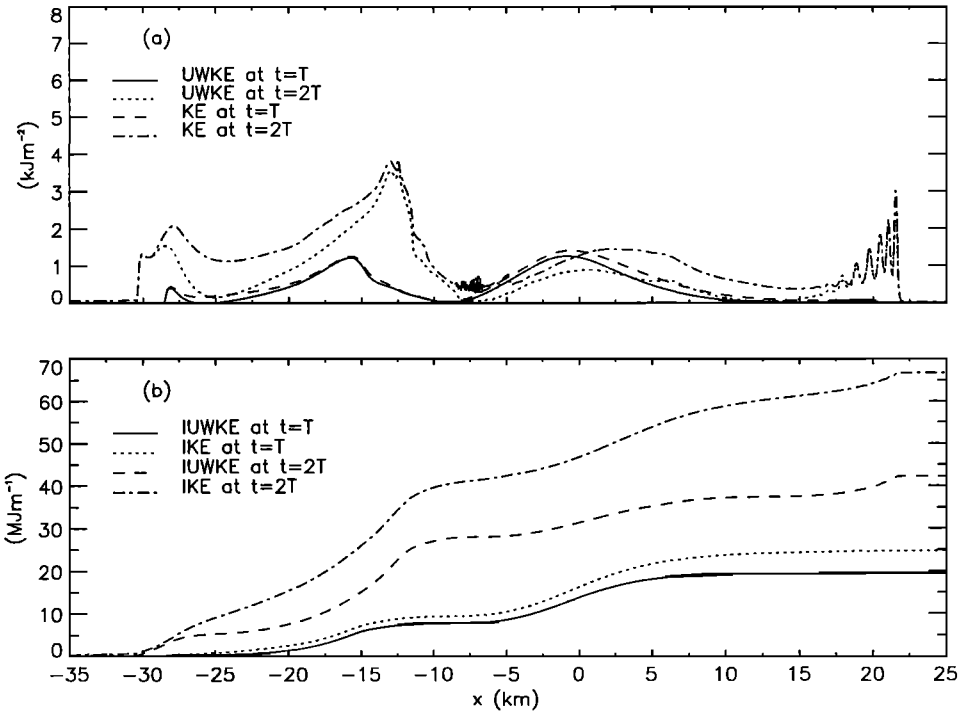

Fig. 14. Kinetic energy. (*a*) Vertically integrated kinetic energy *KE* and the *uw*-kinetic energy *UWKE* after the first and second tidal period as a function of *x*. (*b*) Horizontal integrals integrating from the left boundary.

show that the combined depressions B_1A_2 have a peak value in *APE* which is twice as large as the peak value in A_1 one period earlier. This depression is much wider and contains a total of about 15 MJ m^{-1}. Depression B_2 contains about 2.5 MJ m^{-1}. The undular bore propagating away from the bank edge contains about 11 MJ m^{-1}.

UWKE and *KE*, the vertically integrated perturbation *uw*-kinetic energy $(u^2 + w^2)/2$ and kinetic energy $(u^2 + (v - v(x,z,0))^2 + w^2)/2$, are plotted in Figure 14*a* as a function of *x*. They are computed relative to the initial state for which $u = w = 0$. Figure 14*b* shows the cumulative horizontal integration of *UWKE* and *KE*. Since *w* is typically much smaller in magnitude than *w*, $u^2 + w^2 \approx u^2$. Note that except for the long wave features, the kinetic energy in the along-bank velocity component is insignificant compared to that in the cross-bank component. In particular, *UWKE* and *KE* are the same at depressions *A*, *B*, and *C*, except at their trailing

edges. This suggests that the kinetic energy available for mixing is dominated by the cross-bank and vertical components.

After the first tidal period the kinetic energy in depressions A_1 and C_1 is about 0.5 and 0.2 MJ m^{-1}, respectively. Both values are roughly one fifth of the *APE*. *KE* is larger than the *APE* in elevations E_1 and F_1 by factors of about 2 and 12, respectively. The total *KE* over the whole domain is almost 3 times the total *APE*.

After two tidal periods the total *UWKE* and *APE* are about the same, approximately 42 MJ m^{-1}, while the total *KE* is close to 70 MJ m^{-1}. *APE* is again much larger than *KE* in the depressions, being about 3 times larger in the depression B_1A_2 and about twice as large in the undular bore.

5. COMPARISON RUNS: MODEL SENSITIVITY

In this section, results from comparison runs are presented. These runs were done in order to evaluate the importance of the Coriolis terms in the wave generation process (section 5.1) and to test the sensitivity of the results described in section 4 to the topography and tidal strength (section 5.2), the stratification (5.3), the initial phase ϕ (5.4), and the initialization of the along-bank flow (5.5).

5.1. Wave Generation in the Absence of Rotation

We first consider the effects of the Coriolis term by rerunning the base case with f set to zero. After one tidal cycle there are three pronounced features (Figure 15). Two depressions, one on top of the bank (*A*) and one in the deep water off the bank (*C*), are propagating away from the bank edge. There is also a broad elevation of the isopycnals over the bank edge (*E*). Superimposed on the broad elevation is a small mode-two wave at $x \approx$ -10 km, the same location of the corresponding feature in the rotational case. It is difficult to classify the wave structure between about -20 and -10 km. The relatively flat region of the upper level isopycnals was formed at about $t = 0.5\ \tau$ and has simply been getting longer as the leading depression propagates away, showing the nondispersive nature of the wave.

The differences between the nonrotating and rotating (Figures 15 and 6*h*) cases are striking. In the nonrotating case, depression B_1 is missing due to the nondispersive nature of the response. The response in the nonrotating case is much stronger, due to the fact that rotational effects inhibit the conversion of the potential energy into kinetic energy. That is, if $f \neq 0$, an unforced initial depression evolves to a final state comprised of a smaller depression in geostrophic balance with the along-bank velocity field (see Figures 9 and 10). This results in strong depressions *A* and *C* in the nonrotating case, and hence the elevation over the bank edge formed during the on-bank flow is much bigger (the fluid volume under a given isopycnal is the same in both cases).

5.2. Sensitivity to Topography and Tidal Strength

The size of the depression formed over the bank edge during the off-bank flow is largely governed by the net change in fluid volume (in the computational domain) under a given isopycnal. During the off-bank flow the fluid volume below an isopycnal which has an undisturbed height z decreases by

$$\Delta V = \frac{2z}{\omega} U_{max} \frac{260 - z_b}{260}, \quad \text{if } z < z_b \tag{25a}$$

and

$$\Delta V = \frac{2z_b}{\omega} U_{max} \frac{260 - z}{260}, \quad \text{if } z > z_b. \tag{25b}$$

where z_b is the z level of the bank top. When $z = z_b$, ΔV has its maximum value

$$\Delta V_{max} = \frac{2U_{max}}{\omega} \frac{z_b(260 - z_b)}{260}. \tag{26}$$

An estimate of the effects of changing U_{max} and the topography on the size of the initial depression formed during the off-bank flow can be obtained as follows. Suppose the depression, as measured by the isopycnal at $z = z_b$, formed during the off-bank flow has a characteristic length L and depth D. Then its characteristic volume LD is given by (26). The width of the depression is determined by the width of the bank edge and hence is inversely proportional to the width parameter d. Thus we expect that

$$D \sim U_{max} d \tag{27}$$

and the slopes of the sides of the depression to behave like

$$\frac{D}{L} \sim U_{max} d^2. \tag{28}$$

Thus the depth of the depression is expected to scale with both U_{max} and d, the width is independent of U_{max} and scales with $1/d$ and the tendency to break, or for waves to steepen into jumps, is expected to scale like U_{max} and d^2.

As an example, consider the lowest contour in Figure 6. Its rest height is at $z \approx 216$ m. At $t = 0.25\ \tau$ the lowest point on this

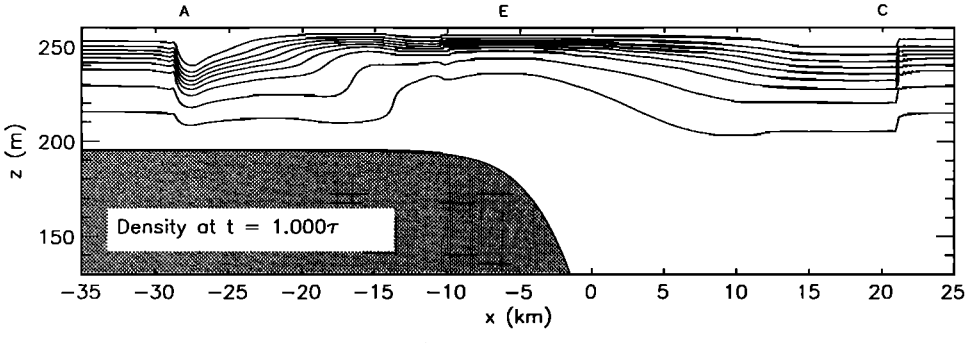

Fig. 15. Contour plot of the density field after one tidal cycle for a case with $f = 0$. All other parameters as for the base case.

contour is at $z \approx 188$ m, so it has gone down by about 28 m. In model sensitivity runs with d increased by factors of 1.5 and 2 the displacement of this contour increased by factors of 1.46 and 2, respectively. Holding d fixed at its base value and increasing U_{max} by factors of 1.5 and 2 increases the displacement by factors of about 1.53 and 2, respectively. At $t = 0.5\ \tau$ the contour is displaced by about 46 m in the base run. Increasing U_{max} by factors of 1.5 and 2 results in an increase in the displacement by factors of 1.48 and 1.87, respectively. When d is increased by a factor of 1.5, the displacement increases by a factor of about 1.43. When d is increased by a factor of 2, a hydraulic jump forms just off the bank edge and overturning occurs. This verifies the increased sensitivity of the slope of the isopycnals to d compared to U_{max} as in (28).

Equation (26) can also be used to estimate the effects of changing the deep-water depth. Changing the deep water depth from 260 m to 320 m increases ΔV_{max} by a factor of (260/320)(255/195) = 1.0625. This small change explains the insensitivity of the results to the increase in the deep-water depth from 260 m to 320 m referred to in section 3.

5.3. Sensitivity to the Stratification

One stratification similar to ρ_1 was used with no significant differences in the results. It had slightly slower wave propagation speeds, so that the second depression formed during the first tidal period was advected right back over the bank edge and disappeared into the initial depression formed during the off-bank flow of the second tidal period. In this section we concentrate on the model results obtained using the deep-water stratification $\rho_2(z)$ given by (8) (see Figures 3, 4 and 5). In this case a very different behavior occurred.

Using ρ_2 as the initial density field and the base topography and tidal strength, overturning occurs before the end of the off-bank flow at $t = 0.5\ \tau$. This is a result of the fact that the topography has a critical slope at tidal frequency for this buoyancy profile (i.e., the rays of internal waves with frequency ω are tangent to the slope at some depth). In a motionless fluid, linear theory says that wave energy of frequency σ propagates along rays given by

$$\frac{dz}{dx} = \pm rs(z) \tag{29a}$$

where

$$rs(z) = \left(\frac{\sigma^2 - f^2}{N^2(z) - \sigma^2}\right)^{1/2}. \tag{29b}$$

When the absolute value of the slope of the topography, denoted by $ts(z)$, is close to $rs(z)$, overturning can result because an incident beam of low-amplitude waves is reflected into a narrow beam of high-amplitude waves. The amplitude of the reflected waves approaches infinity as the boundary becomes parallel to the rays, i.e., as $ts \rightarrow rs$. In Figure 16, $ts(z)$ is plotted along with $rs(z)$. The wave frequency is taken as the tidal frequency ω. The ray slopes are shown for the base density profile ρ_1 and for the deep-water density ρ_2. It can be seen that for the base density the topography is far from being critical (the slope would have to be increased by nearly a factor of 4 to become critical). For ρ_2 the topography is critical at depths of about 173 m and 88.5 m ($z = 87$ and 171.5, respectively). It is quite clear then, that the base topography and the ρ_2 density would result in overturning due to critical reflection. Also plotted in Figure 16 is the topographic slope when the width parameter d is reduced to 0.0001575, 70% of the base value. The topographic slope is now barely subcritical. On the basis of this, we may expect that for d less than about 0.0001575, overturning will be greatly reduced. Significant overturning occurs for values well below this, as low as 60% of the base value. This can be shown to be a result of advection of waves by the tidal flow, as on-bank flow reduces the ray slope of on-bank propagating waves.

5.4. Sensitivity to the Initial Phase

Next we turn to a consideration of the sensitivity of the results to the initial phase of the tidal flow. We begin with a model run which is identical to the base case run except that the run commences at the start of the on-bank flow ($\phi = -\pi$ in (12)). Figure 17 shows contour plots of the density field at $t = \tau$, 1.5 τ, 2τ, and 2.5 τ. They should be compared to Figures 6*d*, 6*h*, 6*l* and 6*p*, respectively. The difference in the two cases is striking.

The wave fields over the bank edge at the end of off-bank flow at $t = \tau$ and 2τ are qualitatively very similar to each other: there is a small elevation separating two depressions, one propagating in either direction. The waves are a bit larger at the end of the second tidal period, but otherwise there is little change. In contrast there is a very large change in the wave fields at the end of off-bank flow between times 0.5 τ and 1.5 τ of the base run (Figures 6*d* and 6*l*).

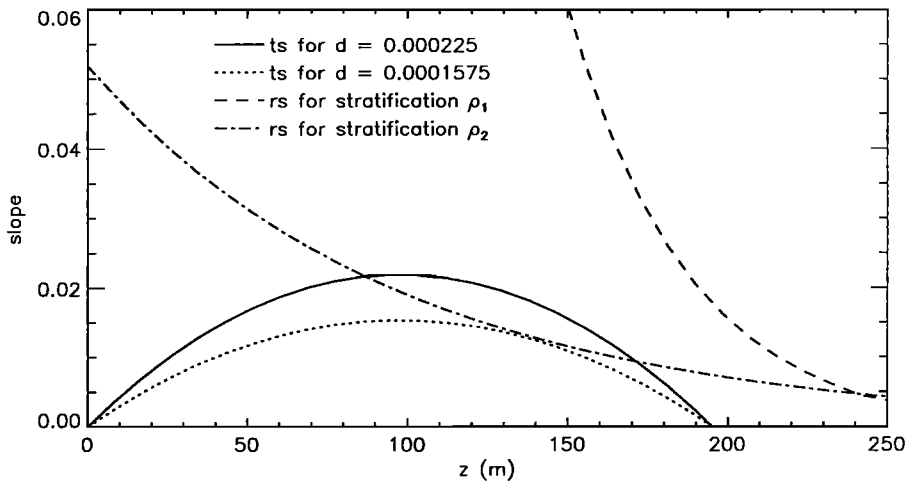

Fig. 16. Topographic slope (*ts*) and the ray slops (*rs*) for the two density profiles.

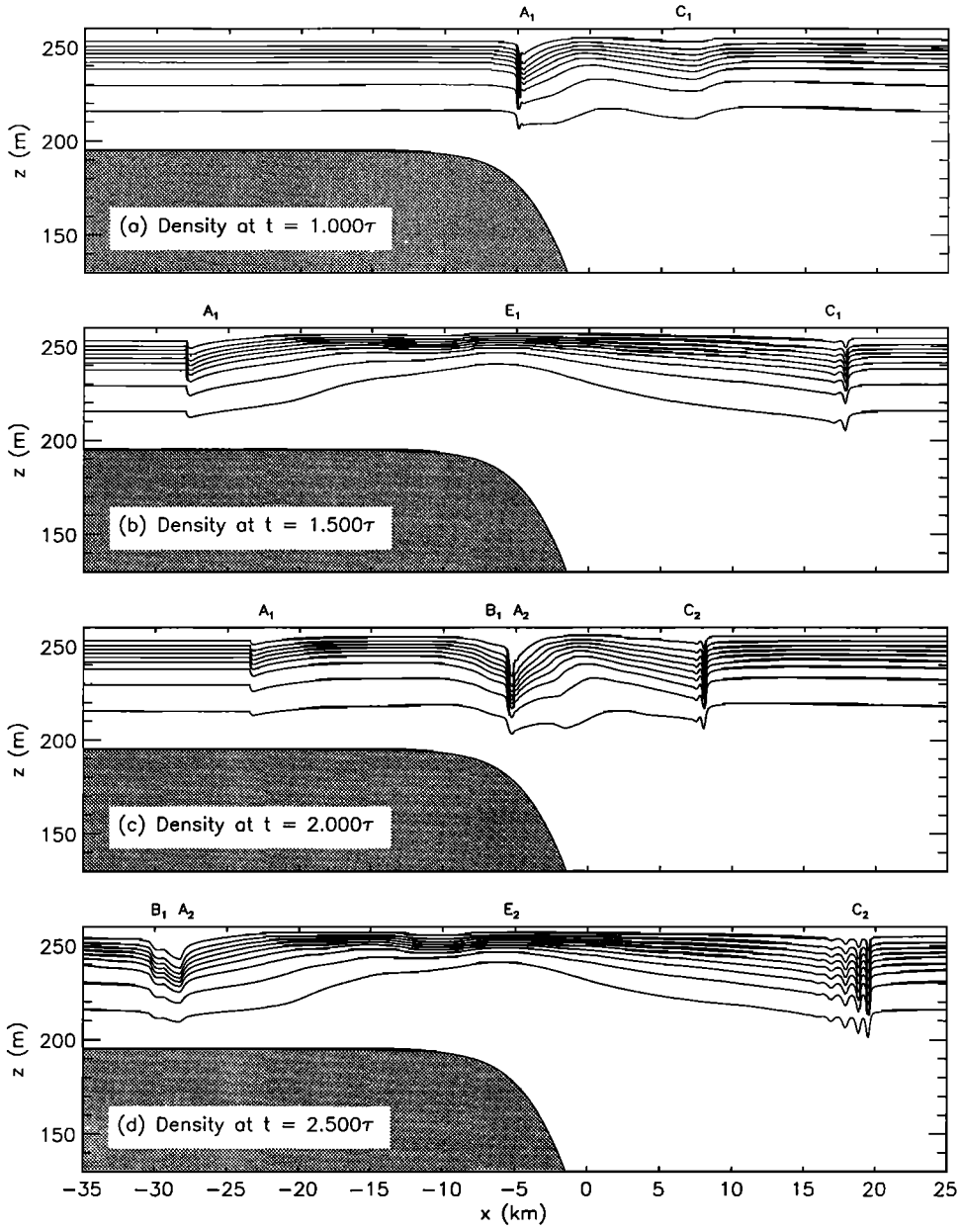

Fig. 17. Density contours using ρ_1 for case initialized at start of on-bank flow ($\phi = -\pi$). Other parameter values unchanged from base case. (*a* and *c*) At the end of off-bank flow. (*b* and *d*) At the end of on-bank flow.

The wave states at $t = 1.5\ \tau$ and $t = 2.5\ \tau$ (Figures 17*b* and 17*d*) are also similar. In contrast, in the base case run there was a significant change in the strength of the response between the ends of the first and second tidal periods (Figures 6*h* and 6*p*; wave B_1 versus B_2 in particular). Another difference between the two cases is the formation (Figure 17) of only one on-bank propagating depression every tidal period, in contrast to the two depressions formed in the base case run.

The differences can be explained in terms of the time varying Froude numbers of the flow and in the differences in the shallow- and deep-water phase speeds. In the present case a large elevation is formed during the on-bank flow. It is farther on-bank than the corresponding depression formed during the off-bank flow in the base run (Figure 6*d*). Because of the slower propagation speeds in the shallow water, the adjustment of this elevation is slower than the adjustment of the depression in the base run. Hence the on- and off-bank propagating elevations generated from this initial elevation have not separated at $t = 0.5\ \tau$ to form a depression corresponding to the elevation E_1 in the base run (Figure 6*d*). For over half of the on-bank flow the Froude number is greater than 1 in water depths of less than 90 m (Table 1), i.e., for $x \leq -4.2$ km, so the off-bank propagating elevation is effectively trapped over the bank edge. During the off-bank flow it is advected off-bank where it partially cancels any depression which might have formed. The advection of the on-bank propagating elevation to the bank edge during the off-bank flow also contributes to this. The asymmetry, whereby the on-bank propagating elevation cannot propagate away from the bank edge but both depressions formed during the off-bank flow in the base case run can, accounts for the qualitative differences between these two cases. U_{max} would have to be greatly reduced to modify this behavior, as the flow in the shallow water is supercritical when $u > 0.34$ m s^{-1}.

An intermediate case initiated at maximum on-bank flow ($\phi = -\pi/2$) was also run. As expected, the elevation formed at the end

of the on-bank flow (t = 0.25 τ) is not as large as for the case initialized at the beginning of the on-bank flow. It again is advected back over the bank edge during the off-bank flow. Because of its smaller size, it does not completely cancel the depression formed during the off-bank flow. The result is a depression which is smaller than in the base case run. Because a depression is formed, two on-bank propagating depressions are generated every tidal period.

These cases also differ in that the barotropic component of the along-bank flow over the bank edge differs at the start of the off-bank flow. The results of the next section indicate that this difference is insignificant.

5.5. *Sensitivity to Initialization of the Along-Bank Flow*

Finally, we consider the sensitivity of the results to the initialization of the along-bank flow v. In particular, if $v(x,z,0)$ is changed, how are $\rho(x,z,t)$, $u(x,z,t)$ and $w(x,z,t)$ affected? Consider one solution of the governing equations, say, the base run, and suppose that $v(x,z,0)$ is changed by adding $V(x,z,0)$ to it. If u, w, and ρ are unchanged at all times, then the pressure will change by an amount P. The changes in v and p satisfy

$$-fV = -P_x \tag{30a}$$

$$V_t + U\cdot\nabla V = 0 \tag{30b}$$

$$P_z = 0. \tag{30c}$$

The first and third of these equations show that we can have a solution if and only if $V_z = 0$. Differentiating (30b) gives

$$V_{zt} + U\cdot\nabla V_z = -u_z V_x + u_x V_z. \tag{31}$$

Thus V_z can remain zero only if $u_z V_x$ is zero. If V_x is nonzero in regions where u_z is nonzero (near the bank edge) then there is no solution satisfying (30). That is u, w, and ρ will be modified. In the early stages of the flow, $u_z << 1$, so that changes in the initialization of v do not affect the early evolution of the wave field. Only after significant vertical shear in u develops will the flow evolution be modified as nonzero u_z tilts vertical vorticity into the x direction. This nonlinear process results in the generation of vertical shear in the along-bank velocity, which tilts planetary vorticity into the along-bank direction and hence modifies u, w, and consequently, ρ. The governing equation for $\varsigma = u_z - w_x$ is

$$\zeta_t + U\cdot\nabla\zeta = fv_z + g\rho_x. \tag{32}$$

The first term on the right represents the production of vorticity through the tilting of planetary vorticity.

The results of some model runs for different initial v are shown in Figure 18. In these cases, v was changed by multiplying the initialization of the base case run by a constant value. Thus initial

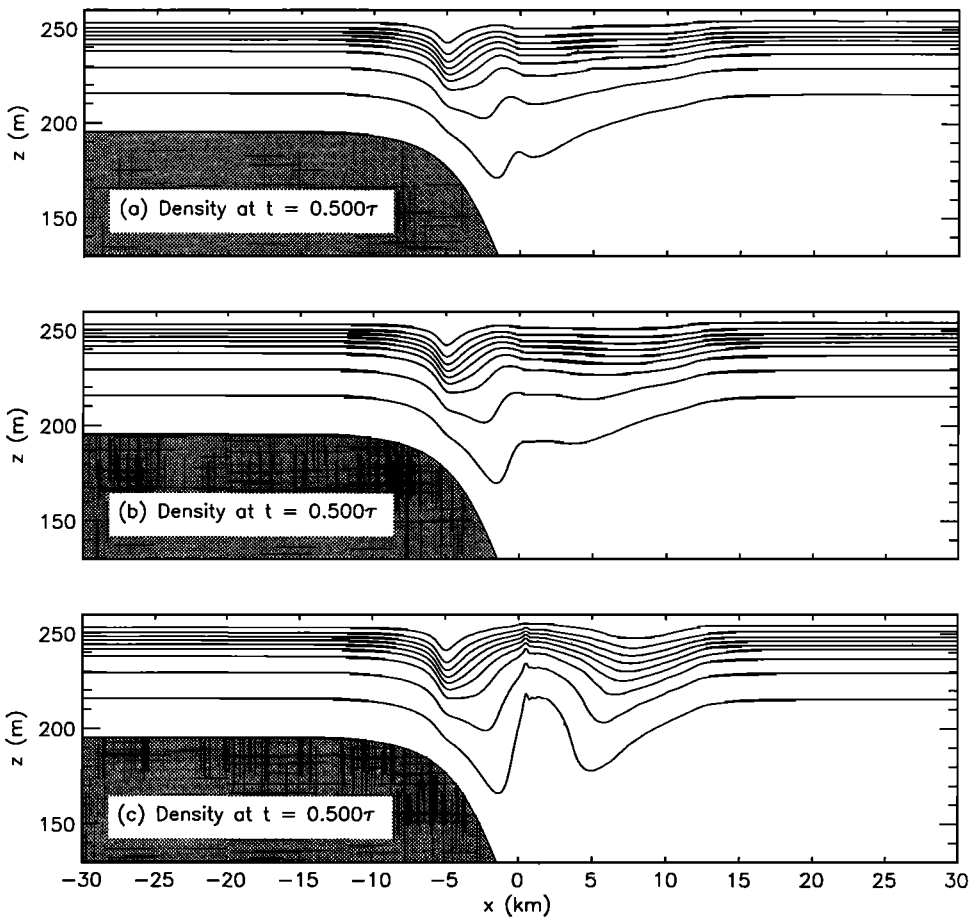

Fig. 18. Density contours at t = 0.5 τ using different initializations for the along-bank velocity v. Other parameter values unchanged from base case. Here the initial v was obtained by multiplying the initialization used in t he base run by (*a*) -1, (*b*) 2, and (*c*) 8.

differences in v_x occur only over the bank edge at $t = 0$. At $t = 0.25\ \tau$ (not shown) there was little change in the model response. Significant u_z have not yet formed to lead to a modification of the wave field. By $t = 0.5\ \tau$ the wave field has been modified. The fluid for which the initial v_x was changed has been advected off-bank. Fluid initially between -6 km and 6 km is now between 1.08 km and 9.35 km. As the large initial values of v_x are contained in this region, we should expect the initial changes in the wave field to occur between about 1 and 10 km at $t = 0.5\ \tau$; u_z is positive in this region with a peak vertically averaged value of about .001 s^{-1} at $x = 1$ km. For positive u_z, (31) predicts that decreasing v_x results in an increase in v_z and consequently, (32) shows that ς increases as well. The model results corroborate this picture. The largest changes occur between 1 and 10 km and are appropriate for the mechanism described. In Figure 18*a* the base run initialization was multiplied by -1. Thus v_x has been increased from the negative values of the base run to positive values and ς is decreased. This results in downwelling at the left side of the modified region. Indeed, for x between about 0 and 4 km the isopycnals are lower than in the base run, resulting in a more pronounced elevation of the isopycnals centred on $x = 0$. In Figure 18*b* the base run v initialization was multiplied by 2. Thus the initial v_x was decreased, resulting in an increase in ς and upwelling. The isopycnals between $x = 0$ and $x = 12.5$ km have been raised slightly. In Figure 18*c* the multiplying factor was 8, resulting in a very large rise in the isopycnals between $x = 0$ and $x = 7$ km and a large drop between $x = 7$ and $x = 12.5$ km.

At the end of one tidal period the major difference between the base run and the case with the initial v multiplied by -1 was that the elevation over the bank edge was much smaller and was centered at about 2.5 km versus -5 km for the base run. When the initial v was multiplied by 2, the only significant difference was that the elevation was a bit larger and centered slightly farther on the bank. In both these cases, depressions A_1, B_1, and C_1 differ only slightly in size and position. This indicates that the base run is one which is insensitive to quite large changes in the initialization of v (i.e., by 100% of the base value). The model run with the initial v multiplied by 8 resulted in strong overturning by $t = 0.625\ \tau$. The short waves seen in Figure 18*c* at about $x = 0$ show that overturning has already commenced at greater depths.

6. SUMMARY AND DISCUSSION

In this paper a detailed description of the nonlinear evolution of the internal wave field generated by tidal flow across a bank edge has been presented. This description was obtained from high-resolution runs of a nonlinear, nonhydrostatic, inviscid numerical model which uses a recently developed method [*Bell et al.*, 1989*a*, *b*; *Bell and Marcus*, 1992]. These idealized simulations are a first step towards understanding the complex phenomena observed in strongly forced regions such as the northern edge of Georges Bank. The model successfully reproduced a number of the observed features, including a large depression resulting in a hydraulic jump during off-bank flow and two on-bank propagating depressions every tidal period. The model also predicts an undular bore propagating away from the bank, a feature which has been inferred from photographs taken from the space shuttle [*La Violette et al.*, 1990].

The base run was started at the beginning of the off-bank flow. During the off-bank flow a large depression is formed over the bank edge, which then undergoes a dispersive adjustment because of rotational effects. The first stage of the adjustment is the generation of two depressions, one propagating in either direction. Because the flow on top of the bank is supercritical during most of the off-bank portion of the tidal period, the on-bank propagating depression is trapped at the bank edge and becomes narrow and deep. The off-bank propagating depression is much broader and weaker. Following the depressions are elevations. After the tide turns on-bank, a second on-bank propagating depression is formed over the bank edge. It initially appears to be a mode-two wave about 8 km behind the first on-bank propagating depression. It eventually evolves into a mode-one depression followed by a mode-two wave. The second mode-one depression is about 15 km behind the first. Horizontal stretching as the fluid is advected onto the bank accounts for about 25% of the increase in the separation distance. The observations are more difficult to interpret, in part because of sampling difficulties (synopticity, resolution) in the more complex physical situation. Figure 9 of *Loder et al.* [1992] shows the formation of the second near-surface depression over the bank edge about 5 km behind the first (after correcting for ship steaming time (J. Loder, personal communication, 1993)). It is first seen when the tide turns on-bank (or perhaps slightly earlier), as in the model results. After it is advected onto the bank, it is about 8 km behind the first depression. The difference in the separation distances could be attributed to the fact that the observed depressions are propagating into water of reduced stratification, so that the first depression is propagating slower than the first. In both the observations and in the model results the distance separating the two depressions just after the second is formed is about half the final separation distance. It is difficult to determine from the observations whether the second depression evolves from an initial mode-two wave as in the model results. The uncertainty of the separation distances and propagation speeds makes this hard to determine; horizontal stretching, rather than differing propagation speeds, could account for all of the increase.

The model results illustrate the importance of rotational effects. Rotation inhibits the conversion of potential energy stored in the large depressions (or elevations) formed over the bank edge into kinetic energy. This greatly influences the size of the waves propagating away from the bank edge (making them much smaller than in the nonrotating case). In addition, long-wave dispersion on a rotating f plane is the cause of the second on-bank propagating depression seen every tidal period. Rotational effects will be important in other locations if the Rossby radius is comparable to, or smaller than, the width of the region of significant topographic slope, and the flow is not restricted by sidewalls. This can be expected to be the case in many open-shelf locations in middle to high-latitudes.

At the end of the first tidal period an elevation over the bank edge is seen. Associated with it is downwelling over the bank edge and upwelling further out. This results in a deeper initial depression during the second period of off-bank flow and consequently in a much stronger response in the second tidal period. In other words, the tidal forcing is almost in resonance with the adjustment of the initial depression formed early in the first off-bank flow period. As a consequence, early in the second off-bank flow period the flow becomes unstable ($Ri < 0.25$) over the bank edge at about $x = 0$ at the bottom. Overturning results in the formation of high-frequency, short waves with horizontal wavelengths on the order of 300 m (Figures 6*m*-6*p*). The instability would be substantially altered if frictional effects were included; however, it is possible that the observed high-frequency waves were produced by a similar instability. The stronger response in the second tidal period also resulted in the nonlinear steepening of the off-bank propagating depression and the formation of an undular bore propagating away from the bank edge

approximately 50% faster than the maximum linear group velocity. The velocity fields associated with the waves are significant fractions of the peak barotropic speeds, confirming the nonlinear nature of the flow field.

The sensitivity studies further elucidate the underlying dynamics. The depth of the initial depression formed during the off-bank flow scales linearly with the topographic slope and with the tidal strength. Increasing the slope results in a narrower deeper depression while increasing the tidal strength results in a deeper depression of the same width. Thus the formation of hydraulic jumps is more sensitive to changes in the topography than to changes in the tidal strength.

The above model runs were carried out using a density profile obtained by averaging data collected just on top of the bank. The density profile was extrapolated into the deeper water in a way which resulted in a very weakly stratified fluid at depths below the top of the bank. For a second density profile, which approximates the observed profile in the off-bank region, the stratification is much stronger at depth and the topography is supercritical to internal waves of tidal frequency between depths of about 173 and 88.5 m. The result is wave breaking by the end of the first off-bank flow period. In model runs with gentler sloping topography, tidal advection results in breaking for slopes well below the critical value. This phenomenon may play a role in maintaining density fronts near bank edges, particularly in situations where the tidal flow is very large, such as Georges Bank. *Marsden* [1986] noted a mixed pocket of fluid at the top of the bank edge (along a different transect) in the location where the topographic slope was critical to the mean density field at tidal frequency.

This study has clarified some of the basic mechanisms responsible for the internal wave field observed at the northern edge of Georges Bank. It is interesting that so many of the parameters are close to critical. Increasing the topographic slope by a factor of 2 results in a hydraulic jump and overturning in the first off-bank flow period. Changing the density field from the mean observations just on top of the bank to one from the deep off-bank water also results in early breaking due to critical reflection of internal waves.

Many physical effects are missing in these idealized calculations. The most important of these are bottom friction, turbulent mixing and the resulting horizontally varying mean density field. A quasi-periodic state also needs to be attained to eliminate the dependence of the response on, for example, the initial tidal phase. Three-dimensional effects could also be important. Frictional effects also result in vertical shear in the barotropic flow and in a vertically varying tidal phase. A more quantitative comparison with the observations is left until these effects have been added to the model.

The physical processes which are included in the model generate internal waves which bear a qualitative and quantitative resemblance to observed ocean features. This illustrates the central role that nonlinear dynamics and rotation can play in the internal wave generation process over finite amplitude topography.

Acknowledgments. This work was funded by grants from the Natural Sciences and Engineering Research Council of Canada and the Canadian Department of Fisheries and Oceans. I would also like to thank John Loder for help with data interpretation, insightful comments during all stages of this work, and careful reading of, and comments on, early versions of this manuscript. Support for consultations with him and other scientists at the Bedford Institute of Oceanography was provided by the (Canadian) Interdepartmental Panel on Energy, Research and Development.

REFERENCES

Baines, P. G., On internal tide generation models, *Deep Sea Res., 29*, 307-338, 1982.

Bell, J. B., and D. L. Marcus, A second-order projection method for variable-density flows, *J. Comput. Phys., 101*, 334-348, 1992.

Bell, J. B., P. Colella, and J. M. Glaz, A second-order projection method for the incompressible Navier-Stokes equations, *J. Comput. Phys., 85*, 257-283, 1989*a*.

Bell, J. B., J. M. Solomon, and W. G. Szymczak, A second-order projection method for the incompressible Navier Stokes equations on quadrilateral grids, paper presented at the AIAA 9th Computational Fluids Dynamics Conference, Am. Inst. Aeronaut. and Astronaut. Buffalo, N.Y., June 14-16, 1989*b*.

Brickman, D., and J. W. Loder, The energetics of the internal tide on northern Georges Bank. *J. Phys. Oceanogr., 23*, 409-424, 1993.

Craig, P. D., A numerical model study of internal tides on the Australian Northwest Shelf, *J. Mar. Res., 46*, 59-76, 1988.

Farmer, D. M., and J. D. Smith, Tidal interaction of stratified flow with a sill in Knight Inlet, *Deep Sea Res., Part A., 27*, 239-254, 1980.

Fornberg, B., and G. B. Whitham, A numerical and theoretical study of certain nonlinear wave phenomena, *Philos. Trans. R. Soc. London, 289*, 373-404, 1977.

Gear, J. A., and R. Grimshaw, A second-order theory for solitary waves in shallow fluids, *Phys. Fluids., 26*, 14-29, 1983.

Gill, A. E, *Atmosphere-Ocean Dynamics*, 662 pp., Academic, San Diego, Calif., 1982.

Hibiya, T., Generation mechanism of internal waves by tidal flow over a sill, *J. Geophys. Res., 91*, 7697-7708, 1986.

Hibiya, T., The generation of internal wave by tidal flow over Stellwagen Bank, *J. Geophys. Res., 93*, 533-542, 1988.

Holloway, P. E., Internal hydraulic jumps and solitons at a shelf break region on the Australian North West Shelf, *J. Geophys. Res., 92*, 5405-5416, 1987.

Huthnance, J. M., Internal tides and waves near the continental shelf edge, *Geophys. Astrophys. Fluid Dyn., 48*, 81-105, 1989.

Lamb, K. G., Numerical simulations of stratified, inviscid flow over a smooth obstacle, *J. Fluid Mech.*, In Press, 1993.

La Violette, P. E., D. R. Johnson, and D. A. Brooks, Sun-glitter photographs of Georges Bank and the Gulf of Maine from the space shuttle, *Oceanography, 3*, 43-49, 1990.

Loder, J. W., Topographic rectification of tidal currents on the sides of Georges Bank, *J. Phys. Oceanogr., 10*, 1399-1416, 1980.

Loder, J. W., and E. P. W. Horne, Skew eddy fluxes as signatures of non-linear tidal current interactions, with application to Georges Bank, *Atmos. Ocean, 29*, 517-546, 1991.

Loder, J. W., D. Brickman, and E. P. W. Horne, Detailed structure of currents and hydrography on the northern side of Georges Bank, *J. Geophys. Res., 97*, 14,331-14,351, 1992.

Marsden, R. F., The internal tide on Georges Bank, *J. Mar. Res., 44*, 35-50, 1986.

Matsuura, T., and T. Hibiya, An experimental and numerical study of the internal wave generation by tide-topography interaction, *J. Phys. Oceanogr., 20*, 506-521, 1990.

Maxworthy, T., A note on the internal solitary waves produced by tidal flow over a three-dimensional ridge, *J. Geophys. Res., 84*, 338-346, 1979.

Pingree, F. D., D. K. Griffiths, and G. T. Mardell, The structure of the internal tide at the Celtic Sea shelf break, *J. Mar. Biol. Assoc., U.K., 64*, 99-113, 1983.

Sandstrom, H., and J. A. Elliott, Internal tide and solitons on the Scotian Shelf: A nutrient pump at work, *J. Geophys. Res., 89*, 6415-6426, 1984.

Smyth, N. F., and P. E. Holloway, Hydraulic jump and undular bore formation on a shelf break, *J. Phys. Oceanogr., 18*, 947-962, 1988.

Wilmott, A. J., and P. D. Edwards, A numerical model for the generation of tidally forced nonlinear internal waves over topography, *Continental Shelf Res., 7*, 457-484, 1987.

K. G. Lamb, Department of Physics, Memorial University of Newfoundland, St. John's, Newfoundland, Canada A1B 3X7

(Received March 10, 1993;
revised July 7, 1993;
accepted August 17, 1993.)